Journal of Palaeosciences 73(2024): 67–91
2583–4266/2024
https://doi.org/10.54991/jop.2024.1874

Rare earth element proxy for distinguishing marine versus freshwater Ediacaran fossils

GREGORY J. RETALLACK

Department of Earth Sciences, University of Oregon, Eugene, Oregon 97403–1272, USA.
Email: gregr@uoregon.edu

(Received 18 February, 2024; revised version accepted 07 May, 2024)

ABSTRACT

Retallack GJ 2024. Rare earth element proxy for distinguishing marine versus freshwater Ediacaran fossils. Journal of Palaeosciences 73(1): 67–91.

Ediacaran fossils and sedimentary rocks are controversial for whether they are marine or non–marine, and this study applies the test of light rare earth over heavy rare earth weight ratios (LYREE/HYREE) to a variety of Ediacaran siliciclastic and carbonate fossil matrices. Holocene soils have light–YREE–enriched arrays (LYREE/HYREE>4.8) and modern deep marine clays have heavy–YREE–enriched arrays (LYREE/HYREE<2.7). Flat arrays of fluvial and shallow marine siliciclastic sediments (LYREE/HYREE 2.7–4.8) are indistinguishable by this proxy. This proxy has been applied to a variety of Ediacaran and Cambrian rocks, for which confounding provenance effects were minimized by comparing marine and non–marine pairs within the same formations. Many samples were within the ambiguous zone (LYREE/HYREE 2.7–4.8), but Ediacaran red beds from Newfoundland, and some beds from China, Namibia, central and south Australia showed diagnostic continental, terrestrial LYREE/HYREE weight ratios of 4.8 to 11.3. A grey tempestite from Newfoundland, a grey sandstone from California, and grey dolostones from Australia and Namibia showed marine LYREE/HYREE weight ratios of 2.7 or less, from the same provenance as terrestrial samples. This new criterion for distinguishing marine from non–marine Ediacaran rocks is supported also by boron content, Ge/Si ratios, and eolian interbeds. Furthermore, new analyses correctly interpreted trilobite and *Cloudina* beds as marine. One surprisingly secure result is that fossiliferous Ediacaran rocks of Newfoundland were not formed in a deep ocean, but on coastal plains. Some fossiliferous Newfoundland beds have LYREE/HYREE weight ratios of as much as 6.0–11.3, found only in paleosols.

Key–words—REE, Ediacaran, Paleosalinity. Vendobionts, Newfoundland.

INTRODUCTION

THE nature of Ediacaran fossils called vendobionts has been a continuing enigma since Seilacher (1992) demonstrated that they could not be the kinds of animals previously suspected. Although there are still proponents for interpreting them as marine invertebrates (Gehling & Droser, 2013; Runnegar, 2022), deep marine xenophyophores are an alternative model (Seilacher *et al.,* 2003), and studies of paleosols have been taken as evidence that they were terrestrial lichens (Retallack, 2013; Retallack & Broz, 2021). A variety of techniques have been applied to discriminating Ediacaran marine and non–marine rocks and fossils: eolian interbeds (Retallack, 2019a; McMahon *et al.*, 2020), desert roses (Retallack, 2022b), caliche (Retallack, 2013), within–bed weathering trends (Retallack, 2013), stable isotopic covariation (Retallack & Broz, 2020), high Ge/Si ratios (Retallack, 2017), and low boron content (Retallack, 2020; Wei & Algeo, 2020). This study develops the use of light versus heavy yttrium and rare earth (YREE) ratios for discriminating marine versus non–marine habitats. Light rare earth enrichment in soil clays was noted from the earliest days of lanthanide studies (Ronov *et al.*, 1967; Duddy, 1980), and has been effectively used to discriminate marine from non–marine chemical sedimentary rocks as old as Archaean (Bolhar *et al.*, 2004, 2005; Bolhar & Van Kranendonk, 2007).

Modern soils, fluvial, and marine siliciclastic sediments each have distinctive arrays of yttrium and rare earth elements (YREE) (Fig. 1). These rare elements have no known biological function, yet are mobilized by metal–scavenging organic ligands within soils (Bau, 1996), by anions and clay in the sea (Lee & Byrne, 1992; Sholkovitz *et al.*, 1994). Soils and granites are enriched in light YREE, with atomic numbers 57–62, rather than heavy YREE, with atomic numbers 63–71 (Fig. 1C). In fluvial systems sediment mixing homogenizes a variety of igneous, metamorphic and soils to more or less flat, normalized arrays (Fig. 1E; Minařík *et al.*, 1998; Bayon *et al.*, 2015; Munemoto *et al.*, 2020). In contrast, deep marine clays have normalized arrays with a positive slope, enriched in heavy YREE over light YREE by alkaline deposition and halmyrolysis (Lee & Byrne, 1992; Sholkovitz *et al*., 1994; Yasukawa *et al*., 2015; Tostevin *et al*., 2016a), compared with shale averages such as PAAS (Taylor & McLennan, 1985; Fig. 1B). Hydrothermal alteration of black smokers on the deep–sea floor creates anomalous concentrations of europium (Fig. 1A; Michard & Albarede, 1986; Hongo & Nozaki, 2001; Sugahara *et al*., 2010; Tostevin *et al*., 2016a). Cerium anomalies can be guides to chemically reducing sedimentary environments (Ling *et al*., 2013; Tostevin *et al*., 2016b; Wu *et al*., 2019). Similar YREE arrays have been found in Archaean (3 Ga) chemical sediments (chert and carbonate) despite metamorphism high in the greenschist facies and near–total cementation and replacement by silica (Sugahara *et al*., 2010; Allwood *et al*., 2010), which substantially diluted overall YREE concentrations (Fig. 1F–I). In summary, heavy YREE are favoured for deposition by local alkaline conditions and basaltic provenance of the deep sea, whereas light YREE are favoured by local acidic conditions and granitic provenance of the land (Jaireth *et al*., 2014). This study uses compiled observations of siliciclastic rocks of known environments to interpret paleoenvironments from the matrix of a variety of Ediacaran fossils.

YREE PROXY FROM MODERN COMPILATION

The use of YREE to distinguish marine and non–marine sedimentary rocks has been based on tipping of normalized arrays toward light or heavy REE (Bolhar *et al*., 2004, 2005; Bolhar & Van Kranendonk, 2007). This paper attempted a quantitative proxy derived from a literature compilation of 471 YREE analyses from a variety of Holocene siliciclastic sediments and soils (Table 1). With the exception of modern deep sea hydrothermal data, none of the Holocene data have large La, Eu, Ce, or Y anomalies from normalized values (Fig. 1), so those environmentally specific anomalies (Taylor & McLennan, 1985; Tostevin *et al*., 2016a, b), are not relevant to this study. Light YREE enrichment is most marked in soils and sediment derived from acidic weathering of granites (Minařík *et al*., 1998), whereas heavy YREE enrichment is found during alkaline deposition and halmyrolitic diagenesis of deep sea clays (Yasukawa *et al*., 2015). There are also strong provenance effects with rivers and turbidites from volcanic arcs very different from those of granitic or mixed sedimentary terranes (Table 1), affirming traditional use of sedimentary YREE as a guide to provenance (Taylor & McLennan, 1985). Oceanic basalts, mantle, and meteorites have low LYREE/HYREE ratios, whereas granites have high LYREE/HYREE ratios (Jaireth *et al*., 2014), so that the difference between deep marine and well drained soil ratios (Fig. 2) also reflects land versus sea provenance.

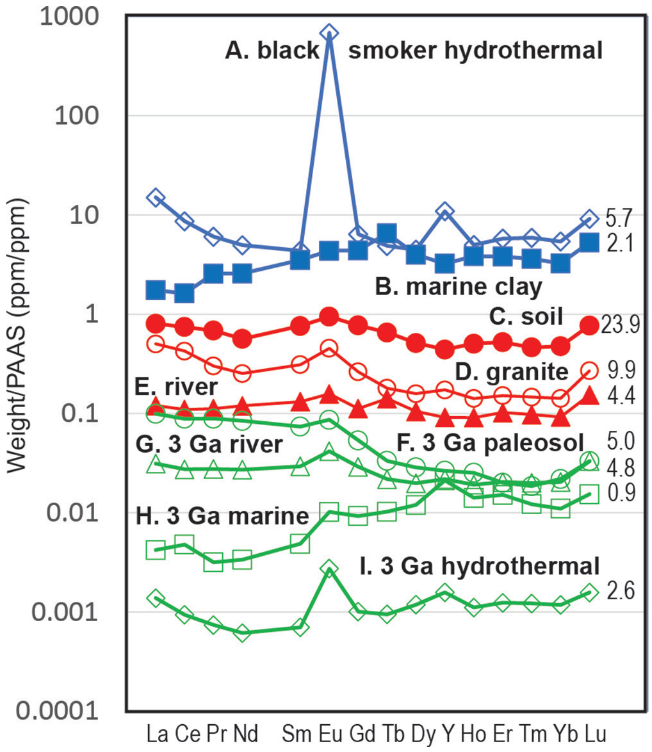

Fig. 1—Source to sink examples of YREE arrays (ppm normalized to PAAS) and LYREE/HYREE ratios (numbers beside arrays) for sediments, soils, and soil–parent monzogranite compared with similar arrays in Archaean (3 Ga) silicified and metamorphosed cherts (Sugahara *et al*., 2010). Distinct slopes and anomalies allow paleoenvironmental interpretation. (A) black smoker hydrothermal vent Iheya Ridge, Okinawa Trough, northwest Pacific Ocean (Hongo & Nozaki, 2001); (B) DSDP site 213 sample 56–57 central Indian Ocean (Yasukawa *et al*., 2015); (C–D) Gleyic Cambisol soil and the monzogranite from which it formed, near Říčany, Czech Republic (Minařík *et al*., 1998); (E) Erdenet River clay, near Erdenet, Mongolia (Munemoto *et al*., 2020); (F–I) samples GFTE3, GFTE1, GW98–1–55, GFSV3 respectively of the Archaean (3 Ga) Farrel Quartzite near Mt Grant, Western Australia (Sugahara *et al*., 2010).

Compiled values in ppm were normalized to Post Archaean Australian Shale (PAAS) values (Taylor & McLennan, 1985) for plotting (Fig. 1). A variety of ways of characterizing the slope of normalized YREE arrays was attempted, but lacked discriminating power. Normalizing YREE arrays is done to minimize the Oddo–Harkins effect of natural variation and visually accentuate anomalies. However, the purpose here was simply to compare two groups of YREE. The most effective discriminator of multiple trials was the

Table 1—Compilation of data for Holocene environments.

Category	Number of analyses	LYREE/ HYREE mean and st. dev.	References
soil	38	5.5 ± 2.7	Minarik *et al*. 1998, Braun *et al*. 1998, Compton *et al*. 2003, Harlavan *et al*. 2009, Sanematsu *et al*. 2009, dos Santos *et al*. 2019
river on continent	94	3.6 ± 0.8	Compton *et al*. 2003, Bayon *et al*. 2015, Munemoto *et al*. 2020
river on volcanics	12	1.8 ± 1.0	Bayon *et al*. 2015
salt pan	29	3.6 ± 0.9	Compton *et al*. 2003, Roy & Smykatz–Kloss 2007
lake	12	3.7 ± 0.8	Das & Haake 2003, Das *et al*. 2008
estuary	78	3.8 ± 0.5	Brito *et al*. 2018
eutrophic marine	40	3.6 ± 0.7	Yang *et al*. 2004, Revillon *et al*. 2011, Anaya–Gregorio *et al.* 2018
oligotrophic marine	77	1.2 ± 0.3	Caccia & Millero 2007
turbidite from continent	15	3.8 ± 1.0	McLennan *et al*. 1990
turbidite from volcanic arc	34	2.8 ± 0.8	McLennan *et al*. 1990
deep sea grey clay	15	1.9 ± 0.3	Yakusawa *et al*. 2015
deep sea red clay	11	1.9 ± 0.1	Yakusawa *et al*. 2015
deep sea hydrothermal	16	1.5	Hongo & Nozaki 2001, Dias & Barriga 2006

simple ratio of non–normalized weights (ppm) of light YREE to heavy YREE, as in the following equation.

$$\frac{LYREE}{HYREE} = \frac{La + Ce + Pr + Nd + Sm}{Eu + Gd + Tb + Dy + Y + Ho + Er + Tm + Yb + Lu}$$

– equation 1

Yttrium (Y) was placed between Dy and Ho based on its effective ionic radius (Bau, 1996). Including Y in the LYREE/HYREE ratio has the effect of biasing interpretation of the arrays towards marine (Fig. 1). This is a simple weight ratio, not a ratio of values normalized to PAAS (Taylor & McLennan, 1985; Bolhar & Van Kranendonk, 2007), nor MUQ (Bolhar *et al*., 2005), nor chondrite (Singh & Manikyamba, 2020). The ratios are reflected in slopes and ratios of normalized values as a part of this work, but that approach was abandoned because yielding only fractional values, whereas simple weight ratios go from fractional to 11 (Table 1). Nevertheless, high LYREE/LYREE weight ratios do correspond roughly to negative slopes on plots of normalized data (Fig. 1). The weight ratio underemphasizes REE, such as Eu, Ho, Tm, and Lu present in small amounts within sediments and soils not hydrothermally altered. Heavier YREE with increased atomic mass form complexes with common marine alkaline anions, unlike acidic soils and rivers where those ions are depleted (Lee & Byrne, 1992; Sholkovitz *et al*., 1994). Use of weight ratios emphasizes the mass effect on fixation, rather than diminishing it. The weight ratio used here is similar to other weight ratios significant for paleosalinity, such as C/S (Berner & Raiswell, 1984), and B/K (Retallack, 2020).

The result of this modern compilation is that deep oceanic sedimentary rocks are distinguished by LYREE/HYREE weight ratios of less than 2.7, and soil environments at weight ratios of more than 4.8 (Fig. 2). Between those extremes rocks may be either marine or non–marine, and show flat REE patterns close to PAAS standard (Fig. 2).

APPLICATION TO EDIACARAN–CAMBRIAN ROCKS

Because YREE elements strongly reflect provenance (Taylor & McLennan, 1985), this study was designed to compare red, plausibly terrestrial, and grey, plausibly marine, beds in the same sequences and thus same provenance, so that paleoenvironmental differences might emerge. Volcanic versus continental source is also evident from petrography of the Ediacaran–Cambrian samples (Retallack, 2013, 2016, 2019 a; Retallack & Broz, 2020; Muhlbauer *et al*., 2020). Most of the samples were from well–known sites for enigmatic Ediacaran megafossils (Figs 3–6), but several Cambrian

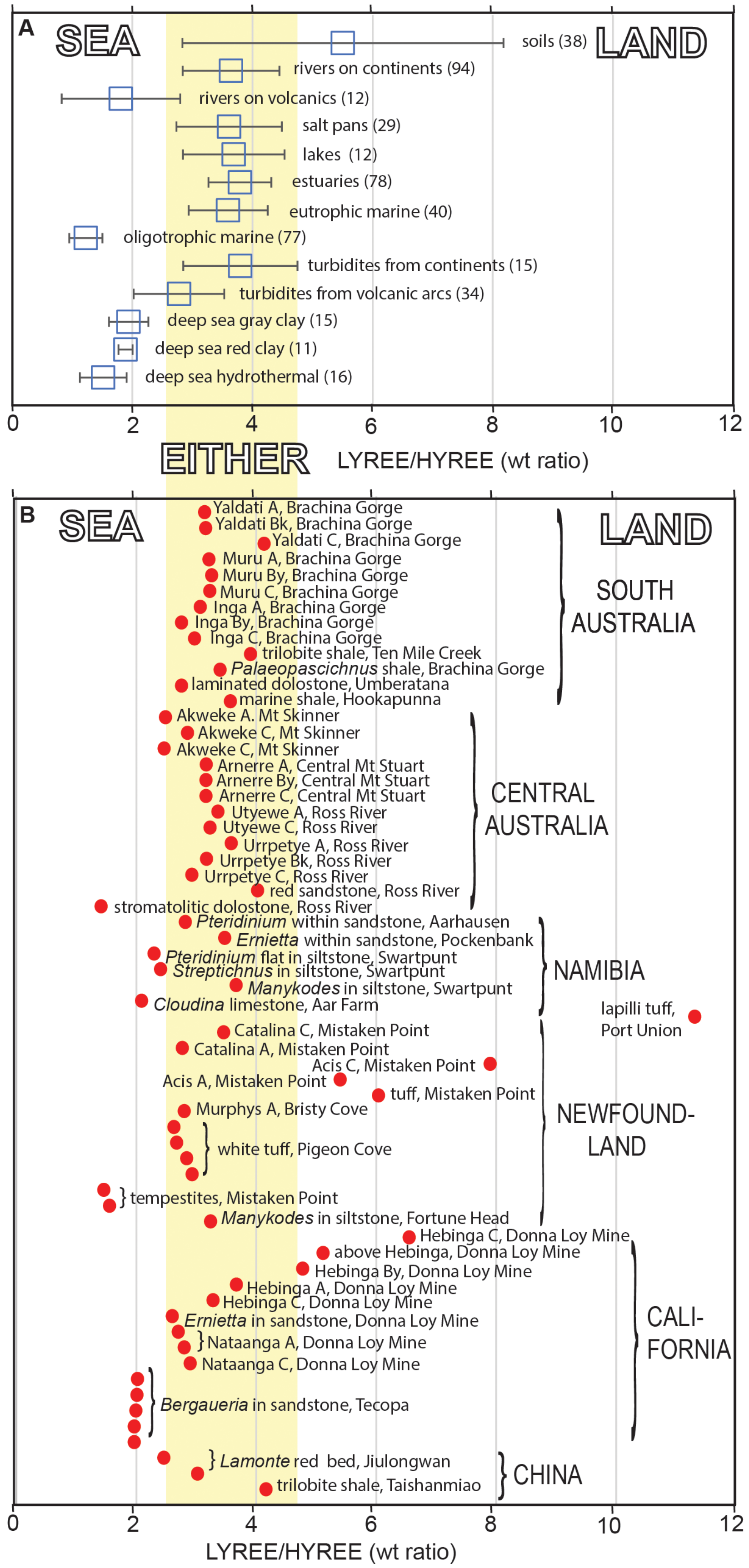

Fig. 2—Comparison of LYREE/HYREE weight ratios of sediments and soils in different Holocene environments (A) and for analyzed Ediacaran and Cambrian rocks and fossils of this study (B). The vertical yellow shaded band are ratios ambiguous for land or sea.

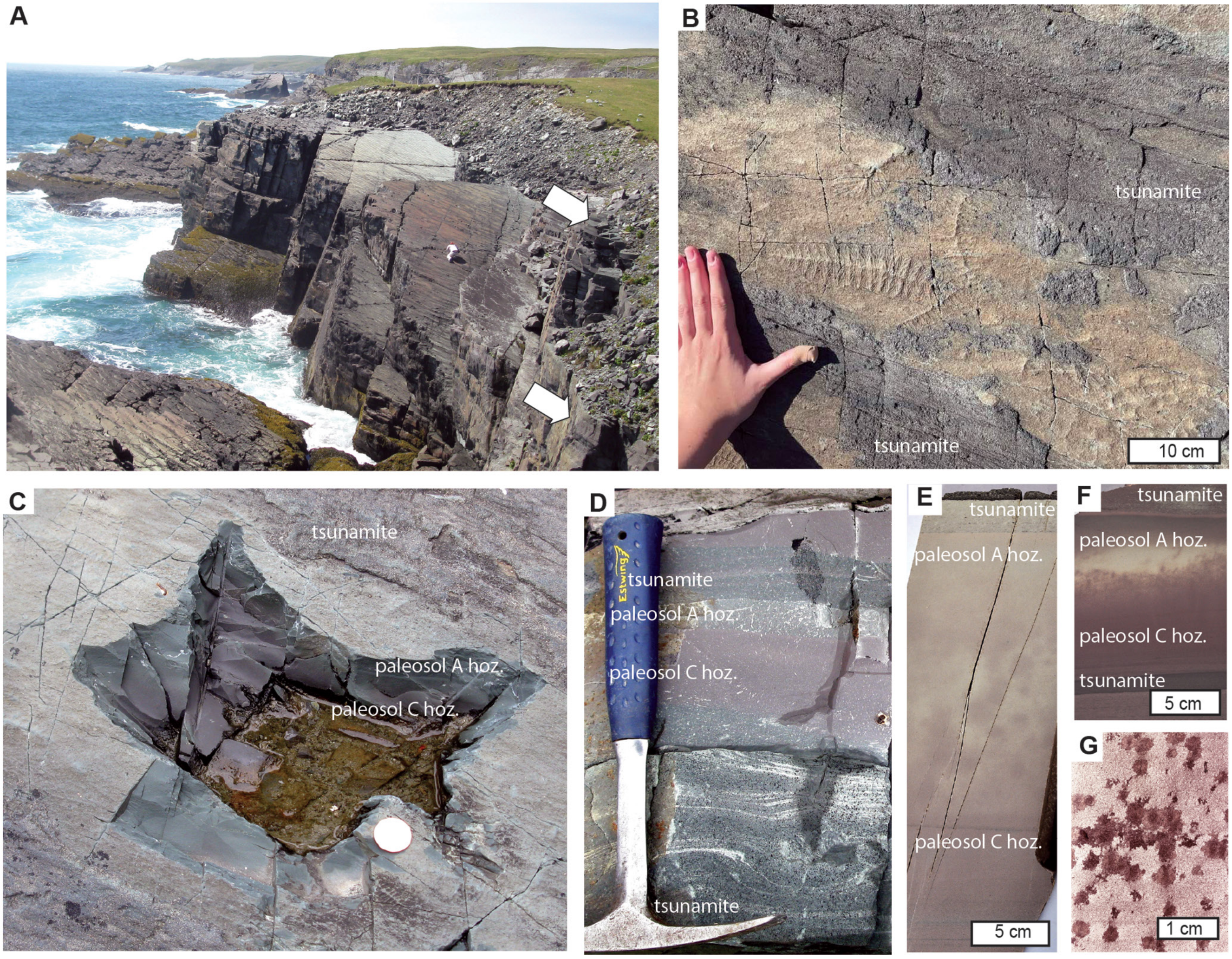

Fig. 3—Ediacaran Mistaken Point Formation in Newfoundland, Canada: (A) Overview of purple fossil surface E at Mistaken Point, with overlying grey shale beds at arrows; (B) *Primocandelabrum hiemalorum* (left) and *Fractofusus misrae* (right) on surface E; (C) illegal collection hole on surface E showing fossils at surface, green–grey reduction of surface and purple subsurface of an Acis bed; (D) cross section of green grading down to purple Acis bed and sharply defined sandstone beds at 7.3 m in section at Mistaken Point; (E) polished slab of Maglona bed at 22.3 m in section at Mistaken Point; (F) polished slab of Acis bed at 9.8 m in section at Mistaken Point; (G) thin section scan of lapilli and scoria tuff specimen R3932 at 8 m in section near Catalina. Named beds and sections are detailed by Retallack (2014, 2016), panel B is courtesy of Cathryn R. Newton, Sarah Tweedt is scale in panel A.

marine shales with trilobites in the same regions were also analyzed (Fig. 7). All the Holocene data and most of the Ediacaran–Cambrian data are for siliciclastic sediments, with exception of three Ediacaran dolostones, which stand out for order of magnitude lower amounts of YREE (Fig. 8D, F, K). All were collected by hammering in the field, then transported and stored dry. Samples of rocks and fossils analyzed here (summarized in Table 2, with full analyses in Tables 3–4) are all archived in the Condon Collection of the Museum of Natural and Cultural History of the University of Oregon (online catalog at http://paleo.uoregon.edu/).

Most of these samples were siliciclastic, and the few dolostone analyses were clayey. Unlike purely chemical sediments which reflect local solutions, clastic rocks also contain YREE evidence of provenance, because these refractory elements represent sediment sources (Taylor & McLennan, 1985; McLennan, 1989). Each local area has unique europium, cerium, or other anomalies, and different overall YREE concentrations, that are carried forward from source to sink (Bau, 1996). For this reason, this study compared marine and non–marine rocks of similar provenance. Sample selection for this study thus included known grey marine

Table 2—Samples analyzed for yree.

Locality	Formation	Fossil or pedotype	Horizon	Depth cm	Sample	Ma	Coordinates	LYREE/ HYREE
Ten Mile Ck, S. Aust.	Oraparinna Shale	*Redlichia*			F114817	512	S31.287879 E138.916839	3.9
Tecopa, California	Wood Canyon F.	sandstone	top	3	R5658	518	N35.889204 W116.07844	2.0
Tecopa, California	Wood Canyon F.	sandstone	middle	7	R5659	518	N35.889204 W116.07844	2.0
Tecopa, California	Wood Canyon F.	sandstone	middle	10	R5660	518	N35.889204 W116.07844	2.0
Tecopa, California	Wood Canyon F.	sandstone	middle	15	R5661	518	N35.889204 W116.07844	2.0
Tecopa, California	Wood Canyon F.	sandstone	bottom	20	R5662	518	N35.889204 W116.07844	2.0
Ross Rr, central Aust.	Arumbera Sands.	sandstone			R5433	520	S23.596572 E134.492300	4.0
Ross Rr, central Aust.	Arumbera Sands.	Urrpetye	A	5	R5437	520	S23.596572 E134.492300	3.6
Ross Rr, central Aust.	Arumbera Sands.	Urrpetye	Bk	30	R5439	520	S23.596572 E134.492300	3.2
Ross Rr, central Aust.	Arumbera Sands.	Urrpetye	C	64	R5442	520	S23.596572 E134.492300	2.9
Taishanmiao, China	Shiujingtou F.	*Coleoides typicalis*			F117755	521	N30.907617 E111.330759	4.2
Swartpunt, Namibia	Spitzkopf Mem.	*Streptichnus narbonnei*			F120826	541	S27.476522 W16.696385	2.4
Swartpunt, Namibia	Spitzkopf Mem.	*Manykodes pedum*			F120827	541	S27.476522 W16.696385	3.7
Hookapunna, S. Aust.	Uratanna Form.	shale			R3528	541	S30.581446 E138.309247	3.6
Fortune Head, Nfdld.	Chapel Island F.	*Manykodes pedum*			F116766	542	N47.074504 W55,859303	3.2
Donna Loy, California	Wood Canyon F.	*Ernietta plateauensis*			F123791A	543	N35.814486 W116.07878	2.6
Donna Loy, California	Wood Canyon F.	Nataanga	A	3	R5356	543	N35.814486 W116.07878	2.7
Donna Loy, California	Wood Canyon F.	Nataanga	A	7	R5357	543	N35.814486 W116.07878	2.8
Donna Loy, California	Wood Canyon F.	Nataanga	C	15	R5358	543	N35.814486 W116.07878	2.9
Swartpunt, Namibia	Felshuhorn M.	*Pteridinium simplex*			F120822	546	S27.477082 W16.695310	2.3
Jiulongwan, China	Shibantan Mem.	*Lamonte trevallis*			F117748	547	N30.815032 E111.077073	1.5
Jiulongwan, China	Shibantan Mem.	*Lamonte trevallis*			F117749	547	N30.815032 E111.077073	3.0
Aar Farm, Namibia	Aar Member	*Cloudina hartmannae*			F120805	549	S26.713174 W16.525328	2.1
Aarhausen, Namibia	Aar Member	*Pteridinium simplex*			F120802	549	S26.720574 E16.535195	2.8
Brachina Gorge, S.Aust.	Ediacara Mem.	Yaldati	A	5	R3205	550	S31.344963 E139.556663	3.1
Brachina Gorge, S.Aust.	Ediacara Mem.	Yaldati	Bk	25	R3207	550	S31.344963 E139.556663	3.2
Brachina Gorge, S.Aust.	Ediacara Mem.	Yaldati	C	40	R3209	550	S31.344963 E139.556663	4.1
Brachina Gorge, S.Aust.	Ediacara Mem.	Muru	A	10	R3215	550	S31.344963 E139.556663	3.2
Brachina Gorge, S.Aust.	Ediacara Mem.	Muru	By	30	R3217	550	S31.344963 E139.556663	3.3
Brachina Gorge, S.Aust.	Ediacara Mem.	Muru	C	50	R3219	550	S31.344963 E139.556663	3.2
Brachina Gorge, S.Aust.	Ediacara Mem.	Inga	A	12	R3229	550	S31.344963 E139.556663	3.1
Brachina Gorge, S.Aust.	Ediacara Mem.	Inga	By	30	R3230	550	S31.344963 E139.556663	2.8
Brachina Gorge, S.Aust.	Ediacara Mem.	Inga	C	40	R3231	550	S31.344963 E139.556663	3.0
Pockenbank, Namibia	Kanies Member	*Ernietta plateauensis*			F120819	550	S27.123739 E16.463789	3.5
Ross Rr, central Aust.	Arumbera Sands.	Utyewe	A	5	R5407	550	S23.594518 E134.491531	3.4
Ross Rr, central Aust.	Arumbera Sands.	Utyewe	C	10	R5408	550	S23.594518 E134.491531	3.2
Mt Skinner, Australia	Grant Bluff F.	Akweke	A	5	R4290	559	S22.24932 E134.307132	2.5
Mt Skinner, Australia	Grant Bluff F.	Akweke	C	12	R4291	559	S22.24932 E134.307132	2.9
Mt Skinner, Australia	Grant Bluff F.	Akweke	C	26	R4292	559	S22.24932 E134.307132	2.5
Central Mt Stuart, Aus.	Grant Bluff F.	Arnerre	A	5	R5160	560	S21.935294 E133.436189	3.2
Central Mt Stuart, Aus.	Grant Bluff F.	Arnerre	By	15	R5161	560	S21.935294 E133.436189	3.2

Central Mt Stuart, Aus.	Grant Bluff F.	Arnerre	C	45	R5163	560	S21.935294 E133.436189	3.2
Mistaken Pt, Newfound.	Mistaken Pt F.	tempestite			R4029	564	S46.626287 W53.163835	1.6
Port Union, Newfound.	Mistaken Pt F.	lapilli tuff			R3932	565	N48.506842 W53.061619	11.3
Donna Loy, California	Stirling Quartzite	Hebinga	above	–7	R5351	565	N35.813181 W116.08137	5.1
Donna Loy, California	Stirling Quartzite	Hebinga	A	4	R5352	565	N35.813181 W116.08137	3.6
Donna Loy, California	Stirling Quartzite	Hebinga	By	7	R5353	565	N35.813181 W116.08137	4.7
Donna Loy, California	Stirling Quartzite	Hebinga	C	11	R5354	565	N35.813181 W116.08137	6.6
Donna Loy, California	Stirling Quartzite	Hebinga	C	15	R5355	565	N35.813181 W116.08137	3.3
Mistaken Pt, Newfound.	Mistaken Pt F.	tempestite			R4025	565	N46.62468 W53.164122	1.6
Mistaken Pt, Newfound.	Mistaken Pt F.	Catalina	A	3	R3995	565	N46.62468 W53.164122	2.7
Mistaken Pt, Newfound.	Mistaken Pt F.	Catalina	C	7	R3996	565	N46.62468 W53.164122	3.5
Mistaken Pt, Newfound.	Mistaken Pt F.	Acis	A	2	R4007	565	N46.62468 W53.164122	5.2
Mistaken Pt, Newfound.	Mistaken Pt F.	Acis	C	8	R4009	565	N46.62468 W53.164122	7.9
Mistaken Pt, Newfound.	Mistaken Pt F.	Maglona	C	12	R4012	565	N46.62468 W53.164122	4.6
Umberatana, S. Aust.	Wonoka Form.	laminated dolostone			R3651	565	S30.23542 E139.122242	2.8
Brachina Gorge, S.Aust.	Wonoka Form.	*Palaeopascichnus delicatus*			F115698	567	S31.336495 W138.566726	3.1
Ross Rr, central Aust.	Julie Formation	dolostone			R5403	568	S23.594080 E134.491604	1.4
Pigeon Cove, Newfound.	Drook Formation	white tuff	upper	5	R3980	574	N46.684862 W53.259280	9.4
Pigeon Cove, Newfound.	Drook Formation	white tuff	middle	10	R3981	574	N46.684862 W53.259280	2.6
Pigeon Cove, Newfound.	Drook Formation	white tuff	middle	15	R3982	574	N46.684862 W53.259280	2.7
Pigeon Cove, Newfound.	Drook Formation	white tuff	lower	20	R3983	574	N46.684862 W53.259280	2.7
Bristy Cove, Newfound.	Briscal Form.	Murphys	A		R4032	575	N46.631333 W53.189757	2.9
Enorama Creek, S.Aust.	Brachina Form.	shale			R3500	600	S31.33156 E138.594026	2.1

Ediacaran stromatolites and Cambrian marine shales with trilobites. Grey Ediacaran dolostones also included likely marine tubular fossils such as *Cloudina* (Cai *et al*., 2017) and *Namacalathus* (Zhuravlev *et al*., 2015). In contrast, samples of rocks with Ediacaran quilted fossils of unknown affinities, such as *Fractofusus*, *Charniodiscus* (Retallack, 2014, 2016), *Dickinsonia* and *Arumberia* (Retallack & Broz, 2021) are siliciclastic red beds with YREE array distinct from grey beds within the same sequences and provenance.

Specimens were pulverized, and 0.2 g of powder added to lithium borate flux (0.9 g), mixed well, and fused in a furnace at 1000°C by ALS Chemex, of North Vancouver, Canada. The resulting melt was cooled, and dissolved in 100 mL of 4% HNO_3 and 2% HCl solution. The same acid treatment and borate flux for silicates was used for the two carbonates analyzed, rather than more thorough leaching recommended by Rongemaille *et al*. (2011) and Zhang *et al*. (2015). This solution was then analyzed from inductive coupled plasma by atomic emission spectroscopy for major elements (ICP–AES), with correction for inter–element interferences, and mass spectroscopy (ICP–MS) for trace elements. Loss on ignition was from 1 g heated to 1000°C for one hour. The standard used for comparison was Canadian Certified diorite gneiss SY4 from Bancroft, Ontario. Error bounds were from multiple runs of standards.

Newfoundland

The Ediacaran, Mistaken Point and Drook formations with vendobiont fossils *Fractofusus* and *Charniodiscus* in the Avalon Peninsula of Newfoundland have been interpreted as turbidites of abyssal marine depths (Wood *et al*., 2003; Ichaso *et al*., 2007). Reexamination of these beds in the field and in polished slabs failed to find any characteristic turbidite features: purple rather than grey color (Fig. 3C–G), silty rather than clayey tails (Fig. 3E–F), loess–like granulometry, and sharp sandstone top rather than grain–size grading (Fig. 3D–F). Other features of the beds are evidence of paleosols, such as matrix–supported accretionary lapilli (Fig. 3G) and sanidine crystal tuffs, tau analysis including base and P depletion, and low B content (Retallack, 2014, 2016, 2020). Turbidites in contrast show base enrichment (McLennan *et*

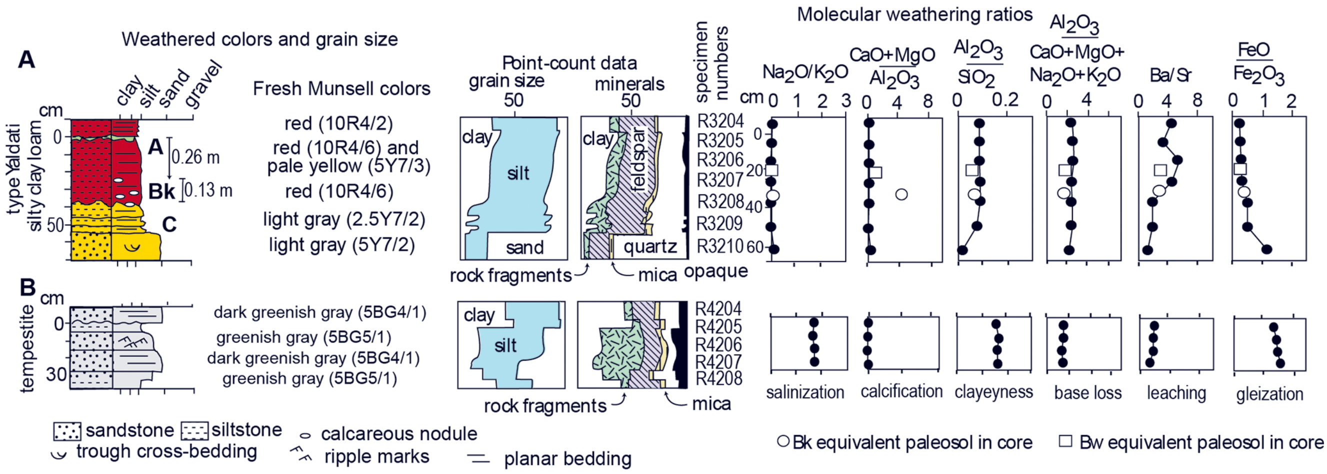

Fig. 4—Chemical and petrographic data on an Ediacaran paleosol from the Ediacara Member in Brachina Gorge, South Australia (from 13.6 m in fig. 1 of Retallack 2013), contrasted with a tempestite from the upper Mistaken Point Formation at Mistaken Point, Newfoundland (63.7 m in fig. 3B of Retallack 2014, 2016).

al., 1990; Korsch *et al*.,1993; Garcia *et al*., 2004; Kiminami & Fujii, 2007). Furthermore, the fossils of *Fractofusus* and *Charniodiscus* are preserved in life position (Fig. 3D) like vegetation mantled by tsunami sands, rather than uprooted into claystone breccia of the erosive bases of turbidites or tempestites (Peters *et al*., 2007; Szczuciński *et al*., 2012). Other unfossiliferous horizons in the Mistaken Point (arrows in Fig. 3A), and overlying and underlying formations, have mineral and chemical profiles very different from paleosols, and represent genuine turbidites and tempestites (Fig. 3B). These Newfoundland formations were deposited in a forearc basin floored by granitic continental basement, rather than deep–sea pillow–basalt and hydrothermally altered crust (King, 1988; O'Brien *et al*., 1996). These divergent interpretations and their implications remain unsettled. Were vendobionts deep marine invertebrates in turbidites and evolutionary precursors of late Ediacaran shallow marine vendobionts (Narbonne *et al*., 2014; Mitchell *et al*., 2015, 2019)? Or were they an early form of terrestrial vegetation in coastal paleosols buried by tsunamite sandstones (Retallack 2016)? Did they absorb deep marine dissolved organic matter (Mitchell *et al*., 2015, 2019), or biologically enhance weathering and photosynthetic productivity on land (Lenton & Watson, 2004)?

South Australia

The Ediacara and Nilpena Members of the Rawnsley Quartzite are red siltstones and sandstones with iconic megafossils such as *Dickinsonia* and *Spriggina* (Figs 4A, 5A, 6A–B), traditionally interpreted as deposited in shallow sea, lagoons, and coastal plain of a passive margin, granitic coast (Mawson & Segnit, 1949; Jenkins *et al*., 1983). Later interpretations emphasized shallow siliciclastic shelf environments that were completely subtidal, based on interpretation of massive sandstones as submarine mass flows and dish structures as evidence of dewatering (Gehling, 2000; Gehling & Droser, 2013; Runnegar, 2022). In contrast a terrestrial interpretation of the red beds came from discovery of desert roses (Fig. 5C) and chemical and petrographic evidence for paleosols (Fig. 4A), as well as eolian interbeds (Retallack, 2019a, 2022a; McMahon *et al*., 2020). Other paleosols with caliche nodules (Fig. 5B) were found in the Ediacaran upper Nuccaleena Formation (Retallack, 2011). These massive redbeds are quite distinct from grey laminated and graded beds of the Brachina Formation (Fig. 5G), and Wonoka Formation (Fig. 5H) within the same Ediacaran succession, considered uncontroversially marine (Retallack, 2020). Vendobionts persisted after the appearance of abundant Cambrian marine burrows in the Uratanna Formation (Jensen *et al*., 1998). The trilobite bearing Oraparinna Shale in Ten Mile Creek (Paterson & Brock, 2007) was also sampled as a securely marine deposit in the same region. There are conflicting interpretations of these fossil localities. Were the vendobionts shallow marine invertebrates without modern relatives, destroyed by the rise of marine bioturbation, then replaced by the Cambrian evolutionary explosion of marine phyla (Briggs, 2015; Wood *et al*., 2019)? Or were they a form of terrestrial vegetation which continued well into the Paleozoic (Retallack, 2018, 2022 b), replaced by the evolution of terrestrial fungi and land plants (Retallack, 2019b; Strother & Foster, 2021)? Did they graze shallow marine microbial mats (Tarhan *et al*., 2017), or biologically enhance weathering and photosynthetic productivity on land (Lenton & Watson, 2004)?

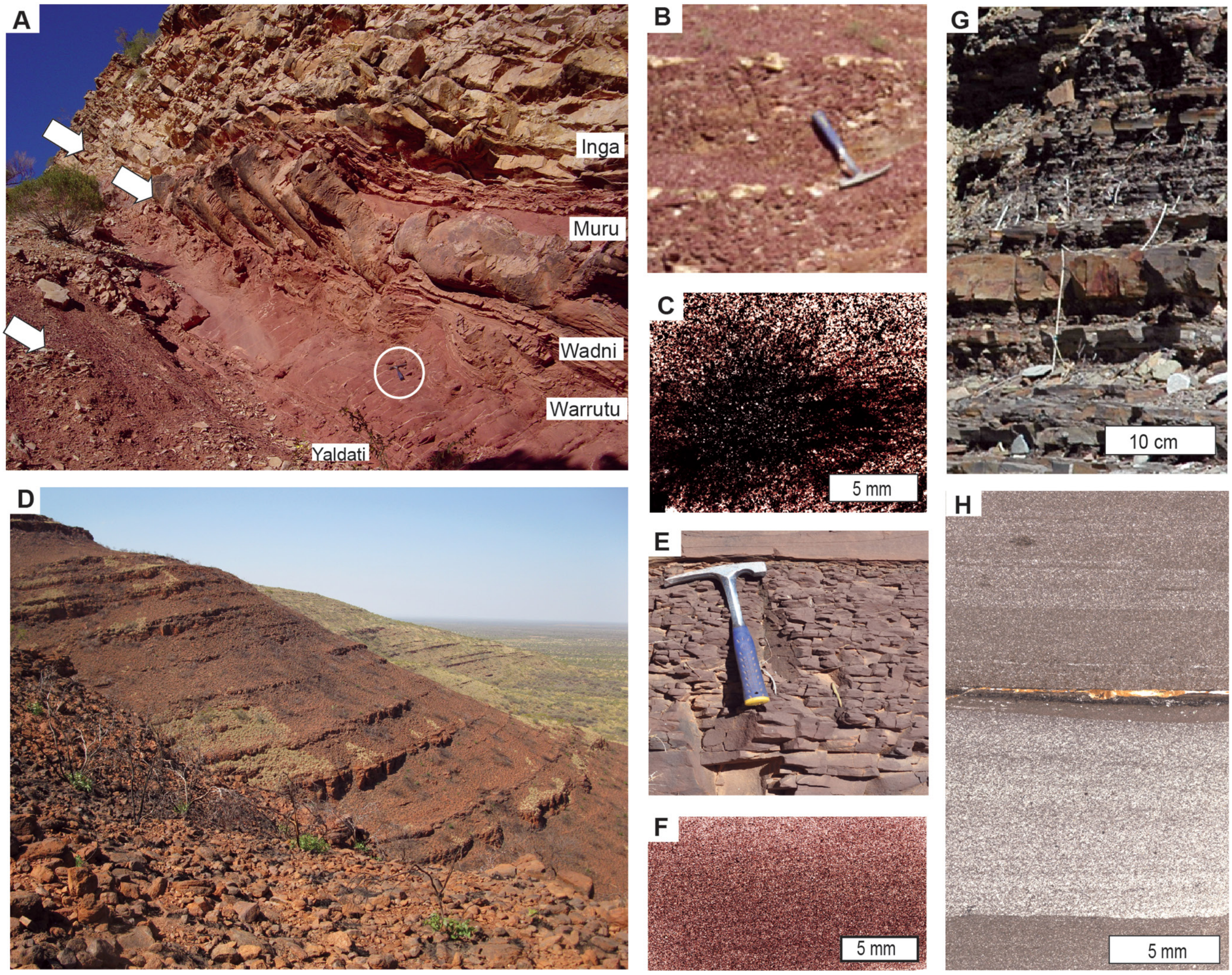

Fig. 5—Ediacaran Ediacara Member of Rawnsley Quartzite (A,C), Nuccaleena Formation (B), Brachina Formation (G) and Wonoka Formation (H) in South Australia, and Grant Bluff Formation (D) and Arumbera Sandstone (E–F) in central Australia: (A) fossiliferous beds (at arrows) in Brachina Gorge (hammer circled for scale); (B) successive calcareous nodular Ika beds in Enorama Creek (hammer for scale); (C) thin section scan (R3229) of gypsum desert rose from Inga bed in Brachina Gorge; (D) overview of red–beds on the southeast spur of Central Mount Stuart; (E–F) profile and thin section scan (R5412) of Atwakaye bed at 192 m in Ross River section; (G) outcrop of Brachina Formation near Enorama Creek; (H) thin section scan (F115701) of shale with *Paleopascichnus delicatus* from Bunyeroo Gorge. Sections are detailed by Retallack (2011, 2013) and Retallack & Broz (2020).

Central Australia

Red beds of the Grant Bluff Formation (Fig. 5D) and Arumbera Sandstone (Fig. 5E–F) in Australia's Northern Territory have unusual, low diversity, megafossil assemblages, including *Arumberia*, *Hallidaya* and *Noffkarkys* (Fig. 6C–F; Retallack & Broz, 2020). These fossils were originally considered cnidarian polyps and medusae in shallow marine sands (Wade, 1969; Glaessner & Walter, 1975), and *Arumberia* has also been considered a microbially influenced sedimentary structure (McMahon *et al*., 2022). Recent evidence for paleosols immediately below these fossils includes petrographic and chemical evidence of clay production, tau analysis of cationic base and P depletion, and stable isotopic covariation (Retallack & Broz, 2020). The *Arumberia–Hallidaya–Noffkarkys* assemblage continues within the same red bed facies well into the Cambrian, above a thick interbed of green–grey siltstone with marine trace fossils including trails of trilobites in the Arumbera Sandstone (Retallack & Broz, 2020). Were these a form of

Table 3—New major element analyses (weight percent).

Locality	Formation	Age (Ma)	Genus/ or pedotype	Horizon/ species	Depth cm	Sample	SiO_2	Al_2O_3	Fe_2O_3	CaO	MgO	Na_2O	K_2O	TiO_2	MnO	P_2O_5	LOI	Total
Ten Mile Ck,	Oraparinna	512	*Redlichia*	*takooensis*		F114817	58.6	17.3	7.53	1.18	3.42	1.04	4.05	0.7	0.09	0.17	7.08	101.23
Tecopa	Wood Cyn	518	sandstone	top	3	R5658	74.1	2.65	1.81	5.92	3.14	0.02	1.23	0.2	0.26	0.27	8.32	98.01
Tecopa	Wood Cyn	518	sandstone	middle	7	R5659	74.9	2.64	1.85	6	3.29	0.02	1.22	0.2	0.26	0.27	8.32	99.07
Tecopa	Wood Cyn	518	sandstone	middle	10	R5660	74.5	2.8	2.01	5.73	3.08	0.02	1.31	0.2	0.26	0.28	8.04	98.33
Tecopa	Wood Cyn	518	sandstone	middle	15	R5661	76.1	2.79	1.94	5.41	2.6	0.01	1.27	0.24	0.23	0.31	7.11	98.11
Tecopa	Wood Cyn	518	sandstone	bottom	20	R5662	79.7	2.89	2.02	5.48	1.19	0.02	1.25	0.25	0.19	0.3	5.71	99.09
Ross River	Arumbera	520	sandstone			R5433	71.1	12.3	3.3	0.94	2.56	0.12	6.36	0.75	0.03	0.19	3.36	101.08
Ross River	Arumbera	520	Urrpetye	A	5	R5437	68.7	10.4	4.91	1.79	2.89	0.12	5.73	0.65	0.17	0.15	4.34	99.93
Ross River	Arumbera	520	Urrpetye	Bk	30	R5439	49.5	8.38	3.91	9.49	7.67	0.1	4.29	0.49	0.15	0.22	15.55	99.8
Ross River	Arumbera	520	Urrpetye	C	64	R5442	24.6	4.14	2.22	21.3	12.8	0.07	2.01	0.27	0.19	0.06	29	96.7
Taishanmiao,		521	*Coleoides*	*typicalis*		F117755	52.4	16.65	6.09	4.26	1.61	0.14	6.68	0.75	0.02	0.15	11.4	100.23
Hookapunna		541	shale			R3528	68.1	13.6	5.26	0.69	2.7	0.9	4.3	0.65	0.19	0.18	4.79	101.44
Swartpunt	Spitzkopf	541	*Streptichnusi*	*narbonnei*		F120826	55.5	10.1	2.83	13	0.96	3.81	0.71	0.39	0.1	0.21	10.95	98.63
Swartpunt,	Spitzkopf	541	*Manykodes*	*pedum*		F120827	69.4	11.65	3.41	5.49	1.12	3.95	0.96	0.41	0.05	0.23	5.17	101.93
Donna Loy	Wood Cyn	542	*Ernietta*	*plateauensis*	1	F123791A	60.9	3.57	4.65	10.65	4.75	0.04	1.68	0.23	0.21	0.13	13.45	100.3
Donna Loy	Wood Cyn	542	Nataanga	A	3	R5356	76.7	3.94	6.39	6.14	1.24	0.05	1.96	0.24	0.21	0.13	3.09	100.14
Donna Loy	Wood Cyn	542	Nataanga	A	7	R5357	83.2	4.13	7.43	2.91	0.28	0.05	2.04	0.31	0.17	0.13	0.74	101.42
Donna Loy	Wood Cyn	542	Nataanga	C	15	R5358	86.8	4.71	4.08	1.67	0.3	0.05	2.26	0.33	0.11	0.15	1.14	101.64
Fortune Head	Chapel Is.	542	*Manykodes*	*pedum*		F116766	63.5	14.75	6.86	2.64	1.97	2.13	1.96	0.82	0.26	0.12	4.9	99.97
Swartpunt	Felshuhorn	546	*Pteridinium*	*carolinensis*		F120822	51.1	11.55	4.2	12.45	1.84	2.16	1.95	0.57	0.2	0.15	11.8	98.11
Jiulongwan	Shibantan	547	*Myxomitoides*	*stirlingensis*		F117748	2.71	0.6	0.36	53.7	0.4	0.08	0.15	0.03	0.01	0.12	42.1	100.49
Jiulongwan	Shibantan	547	*Myxomitoides*	*stirlingensis*		F117749	5.18	0.48	0.35	40.8	10	0.16	0.08	0.02	0.01	0.12	42.8	100.1
Aar Farm	Aar	549	*Cloudina*	*hartmannae*		F120805	2.1	0.59	0.63	53.7	0.57	0.02	0.15	0.02	0.07	0.04	42.4	100.34
Aarhausen	Aar	549	*Pteridinium*	*simplex*		F120802	87.6	2.2	2.05	3.43	0.88	0.07	0.37	0.15	0.03	0.05	4.03	100.88
Brachina Gg.	Ediacara	550	Yaldati	A	5	R3205	80.3	10.4	3.54	0.43	0.62	0.14	2.17	0.57	0.01	0.07	3.23	101.54
Brachina Gg.	Ediacara	550	Yaldati	Bk	25	R3207	78.8	11.05	2.97	0.29	0.65	0.14	2.19	0.61	0.01	0.08	3.43	100.29
Brachina Gg.	Ediacara	550	Yaldati	C	40	R3209	80.5	10.95	1.69	0.13	0.67	0.07	2.28	0.61	0.01	0.04	3.3	100.29
Brachina Gg	Ediacara	550	Muru	A	10	R3215	88.3	5.9	1.6	0.15	0.4	0.07	1.89	0.18	0.01	0.06	1.59	100.21
Brachina Gg	Ediacara	550	Muru	By	30	R3217	86.1	6.84	2.07	0.08	0.39	0.08	2.31	0.29	0.02	0.04	1.58	99.83
Brachina Gg	Ediacara	550	Muru	C	50	R3219	95.3	2.01	1.47	0.07	0.05	0.06	1.04	0.03	0.01	0.03	0.17	100.27
Brachina Gg	Ediacara	550	Inga	A	12	R3229	97.4	2.08	1.12	0.05	0.04	0.05	0.88	0.02	0.01	0.02	0.12	101.81
Brachina Gg	Ediacara	550	Inga	By	30	R3230	94.7	2.5	0.96	0.05	0.03	0.03	0.33	0.02	0.01	0.01	0.66	99.32
Brachina Gg	Ediacara	550	Inga	C	40	R3231	95.6	1.9	1.02	0.12	0.08	0.04	0.3	0.02	0.02	0.01	0.45	99.59
Cent.Mt Stuart	Grant Bluff	550	Arnerre	A	5	R5160	73.9	12.1	5.93	0.08	0.88	0.08	3.28	0.66	0.01	0.04	3.23	100.25

Cent.Mt Stuart	Grant Bluff	550	Arnerre	By	15	R5161	71.8	12.95	6.3	0.09	1.14	0.08	3.61	0.67	0.02	0.07	3.46	100.26
Cent.Mt Stuart	Grant Bluff	550	Arnerre	C	45	R5163	71.8	8.52	4.91	2.61	3.22	0.31	2.24	0.44	0.18	0.09	5.22	99.59
Mt Skinner	Grant Bluff	550	Akweke	A	5	R4290	86.2	6.57	2.64	0.29	0.62	0.08	1.46	0.45	0.01	0.04	2.25	100.66
Mt Skinner	Grant Bluff	550	Akweke	C	12	R4291	85.6	7.54	2.97	0.14	0.79	0.08	1.78	0.47	0.01	0.04	2.29	101.76
Mt Skinner	Grant Bluff	550	Akweke	C	26	R4292	87.8	5.89	2.64	0.15	0.53	0.06	1.3	0.44	0.01	0.03	1.83	100.71
Pockenbank	Kanies	550	*Ernietta*	*plateauensis*		F120819	79.3	9.04	1.83	1.11	0.52	0.81	4.43	0.37	0.02	0.04	1.71	99.33
Ross River	Arumbera	550	Utyewe	A	5	R5407	70.2	13.35	3.72	0.75	2.36	0.6	4.15	0.67	0.07	0.13	4.21	100.27
Ross Rive,	Arumbera	550	Utyewe	C	10	R5408	67.8	13.95	5.54	0.87	2.54	0.55	4.32	0.69	0.04	0.13	4.6	101.09
Mistaken Pt.	Mistaken Pt.	564	tempestite			R4025	64.8	17.6	5.79	0.25	1.55	3.01	3.21	0.85	0.12	0.1	2.69	100.04
Brachina Gg.	Wonoka	565	*Palaeopascichnus*	*delicatus*		F115698	74.3	11.2	3.39	0.73	1.97	1.09	4.15	0.53	0.04	0.16	3.17	100.8
Donna Loy	Stirling	565	Hebinga	above	–7	R5351	92.1	2.98	1.48	0.08	0.19	0.05	1.61	0.38	0.01	0.02	0.29	99.22
Donna Loy	Stirling	565	Hebinga	A	4	R5352	92.2	2.17	2.53	0.06	0.08	0.05	1.29	0.58	0.02	0.01	–0.46	98.55
Donna Loy	Stirling	565	Hebinga	By	7	R5353	91.5	2.76	1.88	0.05	0.12	0.04	1.55	0.65	0.02	0.01	0.02	98.63
Donna Loy	Stirling	565	Hebinga	C	11	R5354	93.2	3.07	1.23	0.04	0.2	0.05	1.63	0.61	0.01	0.02	0.1	101.19
Donna Loy	Stirling	565	Hebinga	C	15	R5355	91.5	3.4	2.81	0.03	0.19	0.05	1.75	0.57	0.02	0.009	–0.43	100.52
Mistaken Pt.	Mistaken Pt.	565	Catalina	A	3	R3995	73.1	13.05	3.37	0.13	1.03	1.66	2.94	0.43	0.07	0.06	2.23	98.16
Mistaken Pt.	Mistaken Pt.	565	Catalina	C	7	R3996	71.8	14.2	3.49	0.18	1.09	1.62	3.28	0.45	0.07	0.06	2.62	98.95
Mistaken Pt.	Mistaken Pt.	565	Acis	A	2	R4007	62.5	18.05	5.98	0.15	1.52	2.76	3.67	0.85	0.11	0.1	2.99	98.78
Mistaken Pt.	Mistaken Pt.	565	Acis	C	8	R4009	63.4	18.05	6.24	0.16	1.63	2.73	3.61	0.85	0.12	0.1	2.85	99.84
Mistaken Pt.	Mistaken Pt.	565	Maglona	C	12	R4012	65.4	17.5	4.45	0.32	1.56	1.75	4.14	0.47	0.1	0.1	3.26	99.16
Mistaken Pt	Mistaken Pt.	565	tempestite			R4029	62	16.95	8.07	0.3	1.86	2.94	2.61	1	0.17	0.1	2.96	99.03
Port Union	Mistaken Pt.	565	tuff			R3932	56.4	11.9	1.92	13.65	0.27	6.37	0.19	0.32	0.4	0.35	9.91	101.74
Ross Rr.	Julie	565	dolostone			R5403	1.06	0.54	0.31	51.3	2.74	0.44	0.03	0.03	0.01	0.08	41.3	98.46
Umberatana	Wonoka	567	dolostone			R3651	27.6	7.17	2.66	31	2.13	0.94	1.41	0.31	0.15	0.11	25.4	98.98
Pigeon Cove	Drook	574	white tuff	upper	5	R3980	56.1	23.1	2.75	1.54	1.93	0.33	6.86	0.48	0.19	0.1	5.9	99.47
Pigeon Cove	Drook	574	white tuff	middle	10	R3981	57	21.9	2.66	1.42	1.76	0.36	6.83	0.48	0.18	0.1	5.89	98.77
Pigeon Cove	Drook	574	white tuff	middle	15	R3982	58	24	2.73	1.02	1.61	0.33	7.15	0.5	0.14	0.09	5.2	100.97
Pigeon Cove	Drook	574	white tuff	lower	20	R3983	52.2	23.6	3.72	2.22	2.7	0.43	6.76	0.51	0.27	0.1	7.27	99.96
Bristy Cove	Briscal	575	Murphys	A	2	R4032	69.3	13.7	4.93	1.54	2.26	2.07	2.84	0.55	0.18	0.07	4.25	101.77
Enorama Ck.	Brachina	600	shale			R3500	74.1	9.91	5.62	0.95	1.52	3.11	1.22	0.88	0.11	0.17	2.1	99.73
Enorama Ck.	Nuccaleena	634	Alpa	A	5	R3516	59.8	15.9	7.47	1.72	3.29	1.36	3.74	1.1	0.03	0.23	5.55	100.23
Enorama Ck.	Nuccaleena	634	Alpa	Bk	40	R3518	29.1	5.62	2.02	19.45	12.95	0.79	1.03	0.24	0.66	0.11	28.8	100.79
Enorama Ck.	Nuccaleena	634	Alpa	C	60	R3519	61.4	16.35	7.45	1.29	3.06	1.33	3.86	1.14	0.05	0.21	5.09	101.28
Enorama Ck.	Nuccaleena	635	Ika	A	10	R3511	18.15	4.75	2.51	23.3	15.6	0.95	0.95	0.3	0.21	0.11	34.3	101.16
Enorama Ck	Nuccaleena	635	Ika	Bw	30	R3512	13.65	3.1	1.58	25	16.55	0.78	0.53	0.13	0.19	0.07	38.1	99.71
Analytical	Error (±2σ)					Error (±2σ)	2.705	0.835	0.395	0.18	0.11	0.13	0.025	0.6	0.22	0.03		

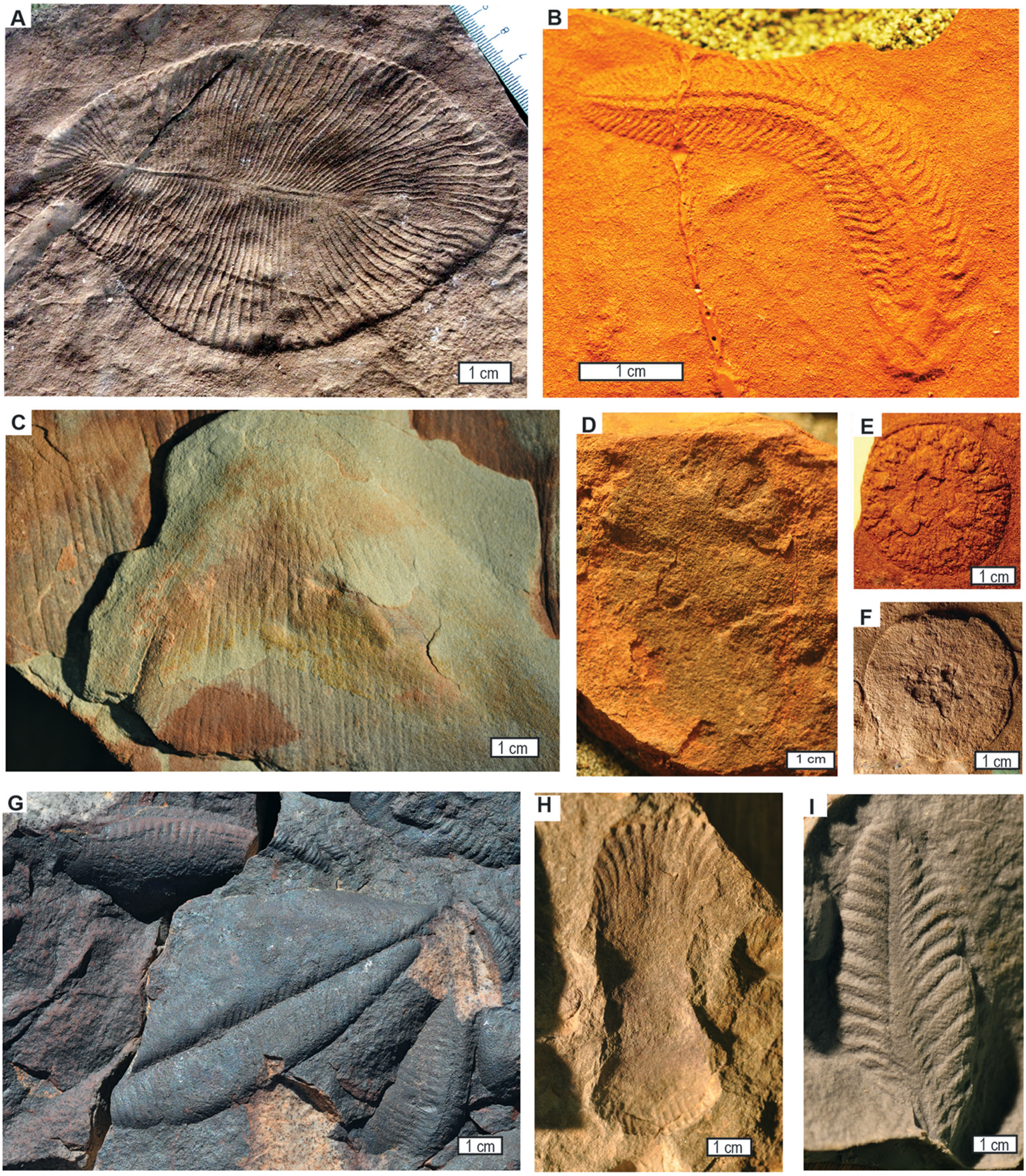

Fig. 6—Ediacaran megafossils: (A) *Dickinsonia costata* from Ediacara Member in the Ediacara Hills, South Australia (South Australian Museum F17462); (B) *Spriggina floundersi* (holotype) from same locality (South Australian Museum F18887); (C) *Arumberia banksi* from Arumbera Sandstone at Valley Dam, central Australia (Geoscience Australia F14948); (D) *Noffkarkys storaasli* from Grant Bluff Formation at Central Mount Stuart, central Australia (University of Oregon F127427); (E–F) *Hallidaya brueri* (holotypes) from Grant Bluff Formation at Mt Skinner, central Australia (South Australian Museum F16478 and 16464 respectively); (G), *Pteridinium simplex* from Kliphoek Member at Aarhausen, Namibia (field photo); (H) *Ernietta plateauensis* from Kliphoek Member on Aar farm, Namibia (Namibian Geological Survey F687); (I) *Rangea schneiderhoehni* (holotype) from same locality (Namibian Geological Survey F193).

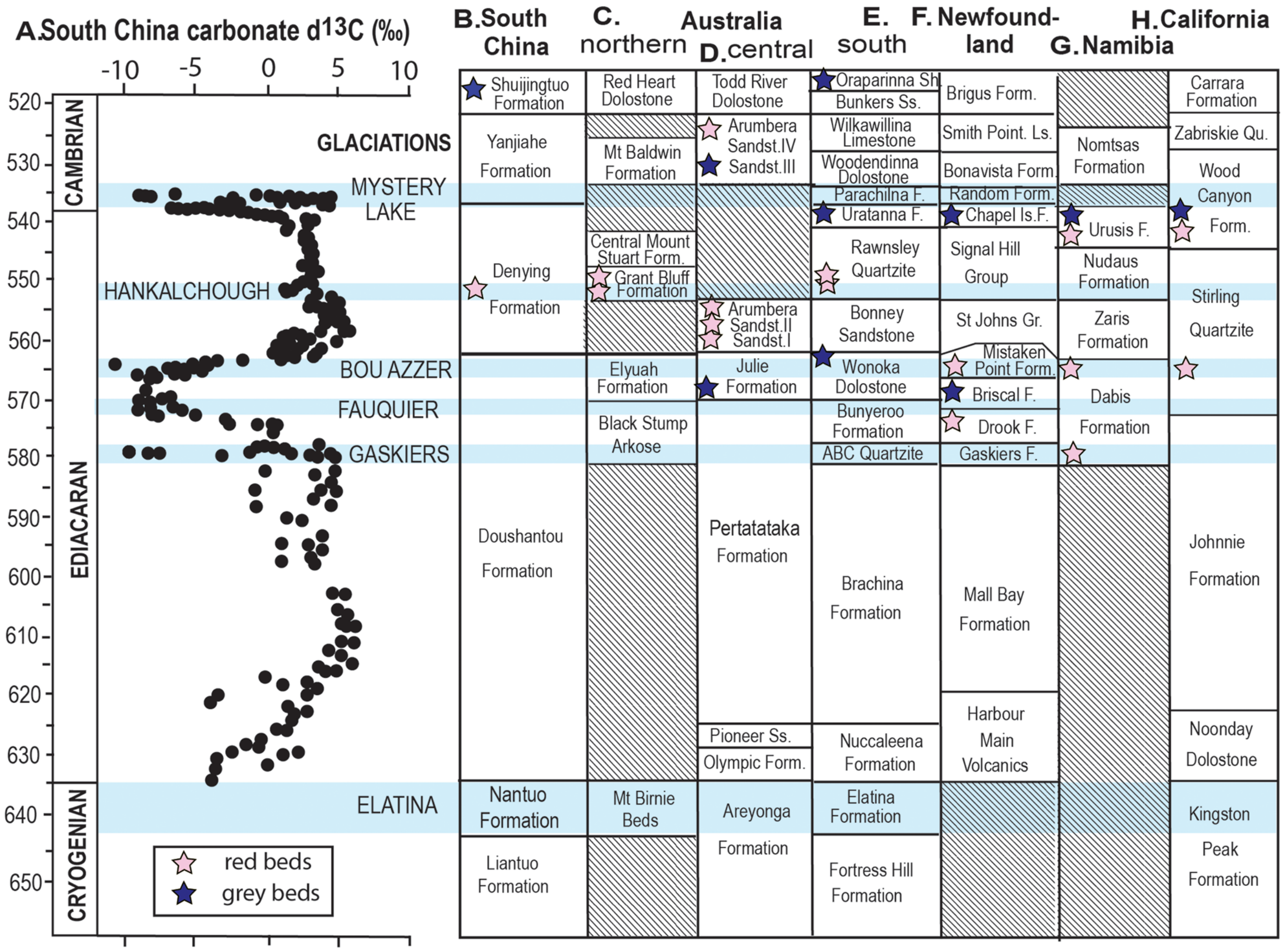

Fig. 7—Stratigraphic position of Ediacaran and Cambrian samples analyzed relative to carbon isotopic chemostratigraphy and named Cryogenian–Cambrian glacial advances: (A) chemostratigraphy from carbonates of the Yangtze Gorge region of South China (Xiao & Narbonne, 2020), scaled to correlation of Gaskiers Glaciation with isotopic minimum EN2, and named glacial advances (Retallack, 2021a); (B) Yangtze Gorges, Hubei, China (Xaio & Narbonne, 2020); (C) western Georgina Basin, Northern Territory, Australia (Retallack & Broz, 2020); (D) eastern Amadeus Basin, Northern Territory, Australia (Retallack & Broz, 2020); (E) Stansbury Basin, South Australia (Retallack *et al.*, 2014); (F) Avalon Peninsula, Newfoundland (Retallack, 2016); (g) southern Namibia (Vickers–Rich *et al.*, 2013); (h) southern California (Smith *et al.*, 2016, 2017).

terrestrial vegetation continuing little–altered from Ediacaran to Cambrian (Retallack & Broz, 2020) until replaced by terrestrial fungi and land plants (Retallack, 2019b; Strother & Foster, 2021)? Did they consume shallow marine microbial mats and other biota (Wade, 1969; Glaessner & Walter, 1975; McMahon *et al.*, 2022), or enrich weathering and productivity on land (Lenton & Watson, 2004)?

Namibia

Mattress–like vendobionts in red beds such as the Kliphoek Member of the Dabis Formation in Namibia include forms such as *Ernietta* (Fig. 6H; Ivantsov *et al.*, 2016) and *Pteridinium* (Fig. 6G; Grazhdankin & Seilacher, 2002), which lived partly buried within the substrate, as well as squat conical forms, such as *Rangea* (Fig. 6I; Vickers–Rich *et al.*, 2013). In contrast grey shales and dolostones of the Mooifontein Member of the Dabis Formation and the Feldshuhorn Member of the Urusis Formation have a very distinct assemblage of tubular fossils such as *Cloudina* (Cai *et al.*, 2017) and *Namacalathus* (Zhuravlev *et al.*, 2015). All of these fossils have been considered shallow marine invertebrates (Grazhdankin & Seilacher, 2002; Ivantsov *et al.*, 2016; Cai *et al.*, 2017), but *Rangea* was found in a paleogully that both flares and has strong sinuosity (Vickers–Rich *et al.*, 2013), more like an intertidal creek than open marine (Davies

Table 4—New trace element analyses (ppm).

Sample	Ba	Ce	Cr	Cs	Dy	Er	Eu	Ga	Gd	Hf	Ho	La	Lu	Nb	Nd	Pr	Rb	Sm	Sn	Sr	Ta	Tb	Th	Tm	U	V	W	Y	Yb	Zr
F114817	457	91	110	12	5.36	3.19	1.29	25	6.18	3.5	1.07	46.6	0.44	13.9	39.6	10.85	180	7.68	5	107	1.2	0.96	18.35	0.47	3.55	127	3	28.2	2.97	118
R5658	412	51.1	20	0.46	5.34	3.16	1.27	2.9	5.96	8.9	1.09	16.5	0.46	4.3	24.2	5.31	31.7	6.51	<1	399	0.4	0.91	5.11	0.43	2.54	18	1	30.2	3.18	367
R5659	454	52.2	20	0.45	5.41	3.34	1.28	2.6	6.43	8.1	1.18	17.1	0.46	3.8	24.3	5.41	31.5	6.36	<1	434	0.4	1.04	4.98	0.44	2.59	20	1	30.9	3.09	349
R5660	449	51.9	20	0.53	5.55	3.21	1.36	3.1	6.52	8.1	1.23	16.3	0.44	3.8	25.9	5.47	33.2	7.14	<1	401	0.3	0.97	5.05	0.48	2.23	18	1	31.2	3.28	342
R5661	432	58.6	30	0.5	6.04	3.69	1.43	3	7.39	9.7	1.31	19.3	0.51	4.7	28.2	6.2	32.8	7.92	<1	547	0.5	1.1	6.75	0.45	2.96	21	1	34.3	3.27	388
R5662	420	57.3	30	0.62	5.7	3.31	1.45	3.1	7.24	10.2	1.24	18.8	0.51	4.7	27.6	5.92	31.8	7.15	<1	442	0.4	1.12	5.68	0.51	2.22	21	1	33.9	3.13	431
R5433	574	106	70	5.01	5.71	3.54	1.23	16.6	6.53	10.4	1.19	54	0.48	16.7	42.8	12.15	148.5	8.35	5	53.5	1.4	0.93	21.6	0.56	3.46	105	3	32	3.32	382
R5437	623	100.5	60	7.88	6.51	3.89	1.45	13.2	7.74	8.7	1.36	47	0.52	14.8	47.1	12.45	158	9.28	4	43.3	1.2	1.18	19.25	0.56	3.26	68	3	33.8	3.35	321
R5439	385	70.1	50	5.94	5.19	2.98	1.08	11.9	5.14	7.1	1.04	34	0.47	11.6	31.5	8.35	128	6.16	4	45.6	1	0.91	15.6	0.44	1.99	54	2	27.2	2.88	257
R5442	196	49.5	30	2.75	3.92	2.33	0.75	5.6	3.96	3.8	0.78	22.5	0.29	6.4	22.3	6.01	60.2	4.33	2	91.8	0.6	0.66	8.2	0.33	1.98	36	1	20.5	2.23	140
F117755	458	70.6	110	13.5	3.86	2.68	0.74	23.5	3.69	4.3	0.85	41.9	0.4	15	27.8	7.89	158.5	4.97	4	182.5	1.2	0.67	15.15	0.42	12.05	173	2	20.9	2.57	164
R3528	636	89.8	80	6.29	5.58	3.17	1.3	20.5	6.15	7.9	1.2	45.4	0.51	15.6	38.2	10.65	145.5	7.17	5	86.9	1.3	1.01	18.1	0.51	3.3	102	15	31	3.14	299
F120826	173	49.5	40	1.6	5.29	2.96	0.93	9.8	5.94	3.7	0.98	25	0.4	7.3	28.3	6.7	33.5	5.98	2	470	0.6	0.89	6.79	0.41	1.93	40	2	27.7	2.53	149
F120827	173	52.6	40	2.22	3.5	2.07	0.72	11.9	4.61	4.2	0.73	23.9	0.28	7.7	28.5	6.91	42.7	5.91	3	468	0.6	0.64	6.78	0.28	1.72	42	2	17.7	1.62	150
F123791A	241	23.8	20	0.59	1.5	0.92	0.41	5	1.67	3.1	0.3	10.9	0.13	2.7	10.2	2.75	38	2.02	1	84.9	0.2	0.27	2.33	0.13	1.58	22	1	9	0.85	111
R5356	339	25.9	30	0.72	1.49	0.85	0.37	5.4	1.75	3	0.28	11.8	0.14	2.7	11	2.95	43.8	2.04	1	97.9	0.2	0.25	2.46	0.13	2.3	17	2	8.3	0.81	109
R5357	282	26.4	30	0.77	1.79	1	0.46	5.9	1.81	4	0.35	12	0.15	3.5	11.5	3.12	45.2	2.38	1	65.2	0.2	0.29	2.9	0.15	1.57	14	1	9.9	0.83	146
R5358	300	32.6	20	0.92	2.23	1.26	0.5	6.2	2.45	4.2	0.44	14.9	0.17	3.8	14.3	3.76	51.5	2.64	2	34.8	0.2	0.37	3.43	0.17	1.46	15	1	13	1.12	152
F116766	365	150.5	70	4.35	12.35	5.81	3.34	17.8	15.95	7.2	2.26	101	0.66	13.6	91.1	22.5	78.7	17.3	3	92.6	0.9	2.08	9.53	0.79	2.13	97	2	70.2	4.63	282
F120822	303	63	60	4.26	6.5	3.79	1.24	14.6	6.33	5.9	1.27	29.6	0.54	10.5	29.8	7.65	87.8	7.5	3	887	0.8	1.03	9.15	0.53	2.65	69	2	35	3.66	223
F117748	28.3	5	10	0.27	0.49	0.29	0.12	0.9	0.41	0.2	0.11	3.6	0.03	0.7	3.1	0.7	5.5	0.48	1	2000	0.1	0.07	0.67	0.05	1.8	11	<1	3.4	0.27	10
F117749	25.3	6.5	20	0.15	0.64	0.33	0.15	0.7	0.81	0.2	0.09	5.3	0.04	0.4	4.1	0.96	3.2	0.75	1	939	0.1	0.09	0.34	0.04	1.12	20	<1	3.4	0.24	6
F120805	41	5.2	10	0.45	0.65	0.26	0.25	0.9	0.52	0.2	0.12	2.3	0.03	0.5	2.4	0.62	6.3	0.69	1	453	0.1	0.09	0.64	0.05	0.96	11	<1	3.2	0.2	6
F120802	83.3	22.3	20	0.57	2.05	1.02	0.38	2.7	1.94	4.6	0.35	10.3	0.14	2.8	10.6	2.61	17.7	2.45	1	99.9	0.3	0.32	2.95	0.18	1.17	13	1	9.8	0.94	183
R3205	463	60.1	50	4.45	4.75	2.82	0.97	12.5	4.54	12.8	0.95	32.9	0.45	13.3	28.8	7.54	96.6	5.51	4	43.6	1.2	0.75	13.85	0.41	2.58	68	2	24.5	2.84	488
R3207	534	59.6	50	4.33	4.78	2.62	0.95	13.7	4.22	12.5	0.96	31.8	0.46	14	27.9	7.36	94.8	5.37	4	47.4	1.3	0.7	14.7	0.45	2.52	71	2	23.8	2.9	475
R3209	268	63.2	50	5.13	3.58	2.35	0.73	15.2	3.25	11.1	0.72	34.1	0.38	14.2	28.4	7.68	99.1	4.89	5	26.9	1.3	0.54	15.6	0.37	2.26	83	2	19.2	2.37	420
R3215	485	26.6	20	2.62	2.06	1.2	0.58	7	1.98	6.3	0.4	14.8	0.17	4	12.5	3.37	76.1	2.4	2	50.5	0.4	0.3	4.76	0.19	1.2	28	1	10.5	1.19	250
R3217	307	31.7	30	3.18	2.48	1.54	0.5	8.8	2.16	9.2	0.53	18.2	0.25	6.4	14.9	4.13	92.5	2.65	2	34	0.6	0.35	7.1	0.25	1.94	33	1	12.4	1.53	362
R3219	302	7.4	30	0.72	0.62	0.26	0.24	2.1	0.82	1.4	0.13	4.3	0.04	0.6	4.2	0.92	39.7	1.09	1	24.2	0.1	0.11	1.82	0.05	0.43	9	1	2.9	0.38	54
R3229	208	7.5	20	0.61	0.63	0.41	0.19	1.7	0.67	1.3	0.13	5.1	0.06	0.6	4.4	1.08	32.7	0.84	1	16.9	0.1	0.12	1.73	0.05	0.38	7	<1	3.4	0.51	49
R3230	171	6.9	20	0.32	0.68	0.36	0.25	2	0.82	1.5	0.12	4.2	0.06	0.5	4.2	0.97	12.5	0.84	1	14.2	0.1	0.11	1.5	0.06	0.33	7	<1	3.4	0.35	54
R3231	317	7.8	20	0.23	0.87	0.39	0.27	2	0.83	1.3	0.13	5	0.06	0.5	4.7	1.19	11.2	0.92	1	19.5	0.1	0.11	1.57	0.05	0.34	11	<1	3.5	0.39	43
R5160	508	75.7	70	9.23	5.17	3.34	0.97	17.5	4.85	9.2	1.16	38.5	0.47	15.5	30.4	8.45	184	6.13	5	13.5	1.4	0.83	15.6	0.51	2.59	105	3	29.8	3.19	334

R5161	581	82.5	80	9.88	6.34	3.44	1.18	18.4	5.54	8.8	1.24	41.1	0.53	15.8	35.1	9.59	208	6.71	5	15.2	1.4	0.94	16.85	0.53	2.89	110	3	32.1	3.54	332
R5163	382	53.3	40	5.1	3.77	2.05	0.85	11.5	4.54	4.9	0.86	26.7	0.32	9.7	24.1	6.27	111.5	4.57	2	45.1	0.8	0.65	9.58	0.27	1.74	69	2	21	2.07	186
R4290	342	44.3	50	3.28	3.84	2.36	0.63	8.3	3.25	8	0.87	22	0.4	9.2	18.5	5.12	71	3.92	3	38.4	0.8	0.62	8.56	0.39	1.79	55	2	22.7	2.67	301
R4291	373	49.9	50	4.08	3.92	2.45	0.74	10.3	3.32	7.7	0.77	24.7	0.36	10.4	21.7	5.76	86.2	3.78	3	46.3	0.9	0.6	9.41	0.35	1.89	62	2	22.2	2.39	285
R4292	239	43.5	50	2.91	3.73	2.53	0.51	7.7	3.42	8	0.91	21.3	0.4	8.7	18.3	4.85	64.3	3.57	3	34.7	0.8	0.57	8.35	0.38	1.86	53	2	22.3	2.41	306
F120819	1405	46.1	30	2.85	3.01	1.89	0.75	10.8	3.31	9.6	0.58	20.5	0.3	6.3	20.2	5.22	220	4.15	2	69.6	0.6	0.51	7.99	0.29	1.99	36	1	14.9	2.16	356
R5407	452	82.1	70	11.1	5.69	3.27	1.16	17.9	5.91	6	1.16	40.5	0.47	14.9	36.6	9.58	167.5	7.23	5	62.8	1.4	0.97	17.85	0.5	2.59	71	3	30	3.25	216
R5408	429	80.8	60	11.25	6.12	3.58	1.21	17.5	6.33	5.9	1.2	40.5	0.52	14.7	37	9.67	175.5	7.83	5	59.5	1.4	0.97	18.2	0.5	2.93	81	4	30.7	3.29	221
R4025	522	33.7	50	4.38	4.27	3.69	0.55	24.3	3.23	7.2	1.08	15.2	0.68	21.3	15.9	4.03	119	3.37	3	64.9	1.3	0.55	11.05	0.64	2.24	109	2	27.7	4.12	272
F115698	504	57.3	50	3.08	3.98	2.48	0.8	13.1	4.14	8.1	0.85	30.1	0.35	10.6	23.9	6.4	116.5	5.07	3	58.5	1	0.71	14.1	0.33	2.92	59	2	20.2	2.28	289
R5351	216	33.5	20	0.44	1.47	0.75	0.32	3.4	1.34	2.3	0.27	17.4	0.09	2.6	12.4	3.61	34.4	1.6	<1	26.5	0.2	0.24	3.72	0.11	0.84	22	2	8.1	0.71	79
R5352	206	17.9	20	0.37	1.08	0.63	0.26	2.3	1	3.7	0.22	9.3	0.12	3.2	7.1	2.04	25.9	1.15	<1	26.6	0.2	0.16	3.84	0.08	0.75	16	2	6.1	0.57	130
R5353	209	27.8	20	0.41	1.28	0.68	0.36	3.2	1.44	3.1	0.25	13.6	0.1	3.6	11.9	3.28	31.8	2.26	<1	22.8	0.3	0.21	4.42	0.12	0.84	23	2	7.2	0.69	112
R5354	217	74.2	20	0.49	2.6	1.39	0.64	3.7	2.68	6.2	0.47	37.5	0.19	8.5	28.4	8.36	35.6	4.5	1	22.7	0.6	0.38	8.95	0.18	1.71	36	5	13.5	1.32	222
R5355	210	24.7	20	0.49	1.67	0.99	0.34	3.9	1.54	3.6	0.34	13.5	0.14	6	9.3	2.73	37	1.68	1	18.8	0.4	0.27	4.75	0.14	1.11	32	5	9.5	0.91	128
R3995	585	60.3	40	4.52	4.71	2.97	1.08	17.4	4.88	4.9	0.99	28.4	0.49	15.1	26.7	7.42	120.5	5.34	2	50.5	1.1	0.75	14.35	0.45	2.98	52	1	26.8	3.21	168
R3996	639	78.8	30	4.87	4.91	3.06	1.27	18.8	5.39	5.3	0.99	37.6	0.5	15.8	34	9.5	129	6.45	2	51.8	1.2	0.81	15.9	0.48	3.13	57	1	27.5	3.24	174
R4007	686	44.8	70	5.66	5.54	3.91	0.8	26.9	4.77	7	1.23	20.8	0.61	17.4	21.9	5.63	149.5	4.63	3	67.7	1.4	0.82	12.05	0.58	1.67	130	2	32.5	4.03	265
R4009	669	56.3	60	5.67	5.62	3.91	0.96	27.1	5.31	7.1	1.26	26.3	0.62	17.9	26.6	7.06	148	5.43	3	68.9	1.3	0.87	11.55	0.58	1.84	130	2	32.6	4.09	259
R4012	776	132.5	40	4.95	4.83	2.62	2.31	25.7	6.91	4.9	0.92	68.9	0.39	10.4	58	15.8	154.5	9.72	3	52.6	0.9	0.9	7.98	0.38	2.13	86	<1	25.4	2.54	184
R4029	386	52.1	80	3.66	9.74	5.01	2.03	22.6	8.65	7.4	1.82	22.8	0.65	18.3	27	6.47	100.5	7.67	3	91.5	1.3	1.5	10.25	0.68	2.04	105	2	44.9	4.55	278
R3932	58.8	77.3	160	0.47	5.62	3.78	1.4	7.4	6.04	6.2	1.21	40.5	0.68	6.9	37.1	9.57	6.4	6.84	2	279	0.5	0.89	8.24	0.58	2.33	7	1	36.8	4.25	226
R5403	13.3	1.8	10	0.05	0.3	0.22	0.09	0.4	0.35	0.1	0.07	1.1	0.03	0.2	1.2	0.28	0.6	0.29	<1	5240	<0.1	0.04	0.19	0.04	1.65	9	<1	2	0.16	4
R3651	356	41.9	50	2.85	3.38	1.77	1.56	10.1	3.66	1.7	0.68	21.7	0.21	6.6	18.9	5	61.4	4.13	2	480	0.5	0.63	6.56	0.3	2.01	55	2	19.8	1.3	57
R3980	1540	152.5	20	7.5	13.1	8.54	1.93	31.5	12.3	11.1	2.84	76.1	1.25	24.4	69.9	18.65	221	13.05	5	28.8	1.9	2.01	23.8	1.27	4.09	44	1	73.8	8.62	386
R3981	1605	161	10	7.9	13.65	8.96	2.1	32.8	12.65	11.7	2.92	80.6	1.31	25.6	74.7	19.9	229	14.3	5	31.4	2	2.07	24.9	1.32	4.2	47	1	77.4	8.68	400
R3982	1625	170	10	8.33	13.5	8.93	2.09	33	12.65	11.4	2.91	83.7	1.31	25.2	77.4	20.8	236	14.45	5	30.5	2	2.07	24.4	1.32	4.26	48	1	75.4	8.89	398
R3983	1515	209	10	8.06	16.5	10.2	2.72	33.5	16.25	12.1	3.4	103	1.4	28.2	96.4	25.9	223	18.05	6	35.7	2.1	2.63	25.9	1.46	4.84	51	1	90.1	9.81	422
R4032	439	610	60	3.88	12.6	5.48	2.81	25.5	23.2	12.2	2.14	336	0.77	71.8	230	66.7	111	33.6	5	90.9	4.5	2.67	14.9	0.77	3.28	35	1	57.4	5	489
R3500	250	58.9	50	1.88	6.9	3.62	1.35	11.1	6.89	9.9	1.27	26.7	0.54	12.6	30.4	7.58	50.3	7.46	3	56.3	1	1.12	13.3	0.53	2.61	76	2	35.4	3.44	363
R3516	335	97.7	100	10.7	7.09	4.24	1.51	22.8	7.73	7.1	1.5	46.8	0.67	18.6	44.1	11.05	174.5	8.44	6	59.1	1.5	1.16	18.95	0.62	3.85	164	3	37.6	4.15	261
R3518	85.3	22.1	30	2.75	3.47	2.39	0.6	7.5	3.28	1.5	0.83	10.2	0.32	4.1	10.6	2.54	47.1	2.45	2	67.9	0.4	0.58	4.21	0.35	1.18	52	1	20.5	2.15	59
R3519	367	99	100	10.75	7.62	4.56	1.52	24.2	7.78	7.3	1.65	47.6	0.65	19.3	44.1	11.55	180	9.08	6	57.4	1.6	1.23	19.35	0.6	4.15	175	3	38.2	4.06	269
R3511	148.5	34.6	30	1.19	2.23	1.24	0.46	7.3	2.26	2	0.43	16.4	0.16	5.3	14.4	3.95	43.9	2.83	2	80.4	0.5	0.33	5.57	0.16	1.66	52	1	10.6	1.09	70
R3512	188.5	14.9	20	0.82	1.74	0.81	0.38	3.9	1.78	0.8	0.32	7.4	0.11	2.4	7.4	1.75	24.9	1.98	1	110.5	0.2	0.31	2.72	0.15	0.91	35	1	8.7	0.83	31
	2	0.2	0.1	0.1	0.03	0.02	0.03	0.5	0.03	0.01	0.01	0.08	0.05	0.8	0.07	0.03	0.5	0.04	3	20	0.04	0.01	0.1	0.01	0.2	1	0.3	0.2	0.2	10

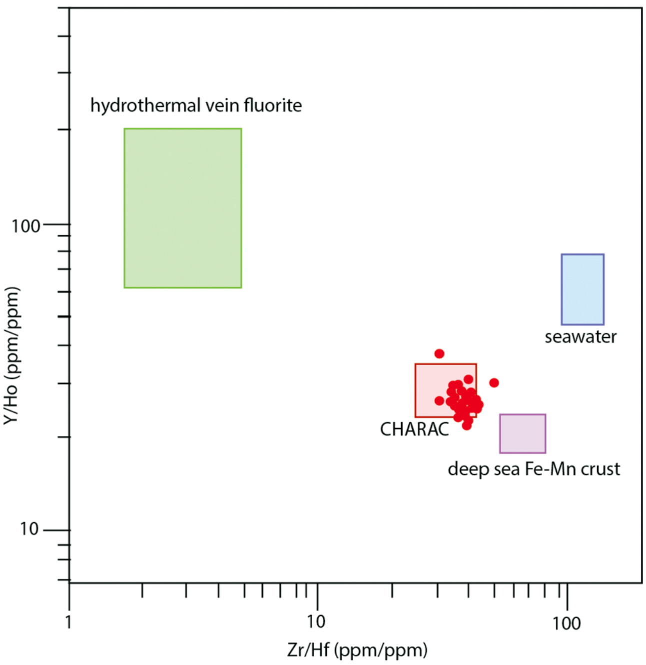

Fig. 8—Continental affiliation from Zr/Hf and Y/Ho weight ratios of all samples analyzed here (closed circles), compared with characteristic continental silicate igneous rocks (CHARAC), deep sea Fe–Mn crusts, sea water, and hydrothermal vein fluorite (Bau, 1996).

& Woodroffe, 2010). Eolian interbeds, massive red beds, and nodules in the Kliphoek Member are more like coastal plain facies (Retallack, 2019a). Were the vendobionts shallow marine invertebrates without modern relatives, destroyed by the rise of marine bioturbation, then replaced by the Cambrian evolutionary explosion of marine phyla (Briggs, 2015; Wood *et al*., 2019)? Or were vendobionts a form of vegetation later replaced by terrestrial fungi and land plants (Retallack, 2019b; Strother & Foster, 2021)? Were vendobionts marine filter feeders or infaunal feeders (Vickers–Rich *et al*., 2013; Ivantsov *et al*., 2016), or did they enhance weathering and photosynthetic productivity on land (Lenton & Watson, 2004)?

California

Ediacaran vendobionts and facies of southern California are comparable with those of Namibia, including *Ernietta* (Smith *et al*., 2017), and *Swartpuntia*, with the latter ranging into Cambrian rocks in California (Hagadorn *et al*., 2000). Vendobionts are found in both the Stirling Quartzite and Wood Canyon Formation, which both have fluvial and marine facies at different stratigraphic levels (Corsetti & Kaufman, 1994; Corsetti *et al*., 2000; Fedo & Cooper, 2001; Muhlbauer *et al*., 2020). The Wood Canyon Formation also includes grey dolostones and shales with *Cloudina* and other small tubular fossils (Smith *et al*., 2016; Selly *et al*., 2020). Were the vendobionts marine invertebrates uprooted by the rise of marine bioturbation (Bottjer *et al*., 2000)? Or were vendobionts an early form of life on land and underground (Retallack, 2013, 2019a)? Were vendobionts marine filter feeders or infaunal feeders (Corsetti & Hagadorn, 2003), or did they enhance terrestrial weathering and productivity (Lenton & Watson, 2004)?

China

Ediacaran Shibantan Member of the Dengying Formation has yielded vendobionts such as *Paracharnia* (Chen *et al*., 2014) and trace fossils such as *Lamonte* (Meyer *et al*., 2014). A small, but diagnostic fragment of *Dickinsonia* also has been reported (Wang *et al*., 2021). These dark grey calcareous shales are usually interpreted as part of an anoxic marine basin (Ling *et al*., 2013; Tahata *et al*., 2013). However, the samples collected for this study in the Jiulongwan section included ferruginized bed tops and pyritic nodular bed bases, associated with flaser bedding, like intertidal facies and gleyed paleosols better known in Ediacaran rocks of Newfoundland (Retallack, 2016). The Cambrian Shiujingtuo Formation was also sampled as definitively marine black shale with trilobites (Zhang *et al*., 2020). Were the Chinese vendobionts enigmatic marine invertebrates replaced by the Cambrian marine biota (Briggs, 2015; Wood *et al*., 2019), or were they a form of intertidal vegetation which continued into the Paleozoic (Retallack, 2018)? Did they graze on microbes or absorb nutrients osmotrophically from sea water (Wang *et al*., 2021), or stabilize intertidal flats against coastal erosion (Retallack, 2018)?

RESULTS AND DISCUSSION

Limitations to YREE as paleoenvironmental indicators

Some limitations to the use of this technique for distinguishing marine from non–marine are clear. The highest marine LYREE/HYREE weight ratio of turbidites from land is 4.8, and lowest non–marine ratio of salt pans is 2.7. Most LYREE/HYREE weight ratios are within this range (Fig. 2), and their arrays are flat and close to PAAS (Fig. 8), so ambiguous for distinguishing fluvial and shallow marine siliciclastic clastic sediments by themselves. An exception is rivers in volcanic terranes which can have LYREE/HYREE as low as 0.8–2.8 (Fig. 2A), and such provenance can be flagged by petrographic and geochemical compositions (Retallack, 2014, 2016).

All the samples analyzed here have igneous (CHARAC) provenance rather than extensive aqueous oceanic, deep–sea Fe–Mn nodular, or hydrothermal alteration, judging from proportions of trivalent to tetravalent rare earth elements of similar charge and radius (Fig. 8). This reflects provenance of these trace elements by weathering and mixing in streams

(McLennan, 1989), supporting the established use of YREE to approximate bulk upper continental crust compositions (Taylor & McLennan, 1985). None of these samples betray prolonged exposure to deep marine or hydrothermal alteration.

Samples with low LYREE/HYREE (2.7–4.8) and flat arrays normalized to PAAS are ambiguous. They may be paleosols, but weakly developed, and other techniques are needed for environmental interpretation, such as interbedded eolian sedimentary structures (Retallack, 2019a; McMahon *et al*., 2020), within–bed geochemical weathering trends (Retallack, 2013), stable isotopic covariation (Retallack & Broz, 2020), high Ge/Si ratios (Retallack, 2017), and low boron content (Retallack, 2020). Thirteen of the samples analyzed here were also included in a recent study of paleosalinity from boron/potassium ratios adjusted for clay diagenesis evaluated in two ways from the ratio of 10 over 10.5 Å values of the illite peak (Weaver index) and width of illite peak at half height (Kübler index) in x–ray diffractograms (Retallack, 2020). These samples plotted against LYREE/HYREE ratios indicate that the red beds analyzed here are indeed non–marine, because the divide between positive and negative $\Delta_{B/K}$ at the threshold between marine and non–marine is near the LYREE/HYREE ratio of 2.7 (Retallack, 2020; Fig. 10).

The expectation of sampling red and grey formations from the same sequences (Fig. 7) was that grey would be marine and red non–marine, as is generally the case for the Phanerozoic sedimentary record (Davies *et al*., 2011; Retallack & Broz, 2020). Phanerozoic marine red beds are known, but are chemical sediments, such as shales and carbonates (Wang *et al*., 2009; Hu, 2013), rather than siliciclastic sediments analyzed here. Holocene oceanic red clays are very different in YREE arrays than all the other samples of this study (Fig. 2). Grey beds with low LYREE/HYREE ratios and positive slope similar to marine sediments (Fig. 1) include Ediacaran dolostones of the Julie and Wonoka formations in central and South Australia (respectively), an Ediacaran tempestite from the upper Mistaken Point Formation of Newfoundland, latest Ediacaran to Cambrian Spitzkopf Member of Urusis Formation in Namibia, Cambrian portion of the lower Arumbera Sandstone with marine trace fossils in central Australia, and multiple levels of a single Cambrian bed with *Bergaueria* and *Wyattia* in the Wood Canyon Formation of California (Figs 2, 7). However Cambrian trilobite–bearing shales from China and South Australia, and grey to white Ediacaran tuffs from Newfoundland lack these marine differentiae, and have instead relatively flat arrays like those found in rivers, coastal plains, deltas, and shallow offshore marine sediments (Fig. 1). Although some trilobites are now known to have invaded estuaries (Mángano *et al*., 2021), this is an unlikely explanation for trilobites in regionally extensive Orarapinna and Shiujingtuo shales analyzed here (Paterson & Brock, 2007; Zhang *et al*., 2020). These marine siliciclastic rocks inherited fluvial YREE arrays like deep sea turbidites (McLennan *et al*., 1990)

Environmental indicators at LYREE/HYREE extremes

Despite LYREE/HYREE weight ratios that are paleoenvironmentally ambiguous, because compromised by provenance, extreme ratios can be diagnostic: especially of soils, oligotrophic marine, deep sea clay, deep sea red beds and deep sea hydrothermal (Fig. 2A). The Holocene oligotrophic marine data are from Florida Bay (Table 1), where terrestrial silicate and nutrient cation input is filtered out by a fringe of mangroves and the waters are clear with little turbidity (Caccia & Millero, 2007). Reconstruction of South Australian Ediacaran rocks as this kind of tropical oligotrophic ecosystem on the cover of a book by Fedonkin *et al*. (2008) is thus unlikely based on data presented here (Fig. 2B). Nor do South Australian Ediacaran rocks show deep sea YREE arrays (Tables 1, 2).

Some of the red bed LYREE/HYREE weight ratios are much higher than 4.8 (Fig. 2B), and their arrays negatively sloped like those of soils (Fig. 8). Especially notable in this regard are the Ediacaran Maglona and Catalina profiles of Newfoundland, and the Hebinga profile of California. The Newfoundland rocks include volcaniclastic sandstones (Fig. 3D) and felsic tuffs (Fig. 3G) among other lines of evidence for derivation from a volcanic arc nearby (Retallack, 2014, 2016), so are extremely anomalous compared with Holocene river alluvium and deep marine turbidites derived from volcanic arcs (Fig. 2A). These new observations support a variety of other lines of evidence (Figs 3–5) that both the siliciclastic and volcaniclastic facies were paleosols (Retallack, 2013, 2016, 2019a). The Hebinga profile of the Stirling Quartzite has pseudomorphs of gypsum desert roses, like other Ediacaran paleosols (Retallack, 2013, 2022a).

Array differences within beds

In cases where multiple samples were taken at decimetric intervals within single beds less than 64 cm thick (Table 2), grey beds showed identical YREE arrays (Figs 2B, 9H, J), whereas individual named red beds showed strong internal differentiation of the bed (Figs 2B, 9A,I,K). In none of these beds was there marked concentration of heavy minerals toward the base, which can affect YREE arrays (McLennan, 1989). The marked differentiation of YREE arrays within single beds is a distinctive feature of soil formation (Minařík *et al*., 1998), and thus marks paleosols, also recognized for these samples from other lines of evidence (Retallack, 2013, 2016, 2022a). Furthermore, the divergence in YREE arrays of different horizons of the same bed is greatest in moderately developed paleosols with sulfate desert roses (By in Fig. 9I) and caliche nodules (Bk in Fig. 9A–B). This effect is especially marked in profiles with sulfate desert roses, formed by acid–sulfate weathering, rather than carbonic acid hydrolysis resulting in carbonate nodules (Retallack, 2013; Retallack & Broz, 2020). Other paleosols with lesser textural and geochemical development due to shorter duration of formation have less distinct YREE arrays within different parts of the same bed.

No anoxic signatures in analyzed samples

None of the specimens analyzed here had significant Ce anomalies, although some are in sequences which include Ce anomalies at other stratigraphic levels (Ling *et al*., 2013; Wu *et al*., 2019). Thus, the samples chosen here for Ediacaran fossils were not from anoxic depositional environments, neither during, nor after deposition. Nor were they from source terranes including igneous rocks with Ce anomalies (Taylor & Maclennan, 1985).

Few hydrothermal signatures in analyzed samples

Positive Eu anomalies were found in dolostones of the Mooifontein Member of the Dabis Formation in Namibia, the Wonoka Formation of South Australia, and the Julie Formation of central Australia, and a negative europium anomaly in a grey Murphys profile from Newfoundland (Fig. 9). The positive anomalies may be evidence of hydrothermal alteration in the dolostones, as in modern hydrothermal systems (Michard & Albarede, 1986; Hongo & Nozaki, 2001), and in Archaean metamorphosed cherts (Sugahara *et al*., 2010). The negative europium anomaly may have been derived from phyllitic metamorphic rocks (Fowler & Doig, 1983), alkali granite, or rhyolite (Beyth *et al*., 1994). The latter is most likely, because the profile in question includes fresh rhyolitic tuff (Retallack, 2014, 2016).

Volcaniclastic versus siliciclastic clastic signatures

Flat YREE arrays in shallow marine and non–marine deposits are similar with LYREE/HYREE ratios around 3, because neither pedogenesis nor marine waters diluted by runoff profoundly modified their fluvial provenance. Shallow marine stromatolitic dolostones (Fig. 9D–F) do have distinctive marine YREE arrays with LYREE/HYREE ratios less than 2.7, less influenced by provenance, and reflecting precipitation of carbonate from seawater. Deep sea shales also acquire HYREE enrichment (Figs 1–2), and would have been apparent in the Ediacaran Mistaken Point and Drook formations, if they were deposited in the deep sea (Wood *et al*., 2003; Ichaso *et al*., 2007). Point counting of the samples analyzed here showed that they had no more than 36 volume percent clay (Retallack, 2014, 2016), and thus lacked the

⟶

Fig. 9—Rare earth element (YREE) analyses (ppm normalized to PAAS) and LYREE/HYREE ratios (numbers beside arrays) of named Ediacaran red beds (left), compared with Cambrian–Ediacaran grey beds with clear evidence of marine conditions in the same area (right): (A) Ediacaran paleosols of the Ediacara and Nilpena Members with *Dickinsonia* and other vendobionts of the Rawnsley Quartzite, in Brachina Gorge, Flinders Ranges (Retallack, 2013); (B) Cambrian Oraparinna Shale with trilobite *Redlichia* (Paterson & Brock, 2007). Ediacaran shale of Wonoka Formation with *Palaeopascichnus* in Brachina Gorge, and laminated dolostone of Wonoka Formation from Umberatana, South Australia (Retallack *et al*., 2014); (C) Ediacaran paleosols of Grant Bluff Formation from Central Mount Stuart, and Mt Skinner, and Arumbera Sandstone from Ross River with *Dickinsonia* and other vendobionts, Northern Territory (Retallack & Broz, 2020); (D) Cambrian siltstones of Arumbera Sandstone Member III with marine trace fossils, and Ediacaran stromatolitic dolostone of Julie Formation from Ross River, Northern Territory (Retallack & Broz, 2020); (E) Ediacaran *Ernietta* from Kanies Member at Pockenbank and *Pteridinium* from Aar Member at Aarhausen, both in Dabis Formation, Namibia (Vickers–Rich *et al*., 2013); (F) drifted and deflated specimen of *Pteridinium* from Feldshuhorn Member, and Cambrian trace fossils *Streptichnus* and *Manykodes* from Spitzkopf Member, all Urusis Formation at Swartpunt; and Ediacaran *Cloudina* dolostone at Aar Farm in Aar Member, Dabis Formation, Namibia (Vickers–Rich *et al*., 2013); (G) Ediacaran paleosols Murphys in Briscal Formation at Bristy Cove, and Murphys in Drook Formation at Pigeon Cove, and others in Mistaken Point Formation at Mistaken Point, Newfoundland (Retallack, 2016); (H) 4 samples of Ediacaran volcanic tuff in Drook Formation at Pigeon Cove, Ediacaran tempestite sandstone in Mistaken Point Formation at Mistaken Point, Cambrian *Manykodes* trace fossil from Chapel Island Formation at Fortune Head, Newfoundland (Retallack, 2016); (I) Ediacaran Hebinga paleosol in Stirling Quartzite near Donna Loy Mine, and other less developed paleosols from Wood Canyon Formation (in background), southern California (Smith *et al*., 2017); (J) 4 successive samples in bed 15 cm thick with marine trace fossil *Bergaueria* and body fossil *Wyattia* in Cambrian Wood Canyon Formation in Emigrant Pass, southern California (Smith *et al*., 2017); (K) ferruginized surface of Ediacaran tidal–flat paleosols (Sulfaquent) with trace fossil *Lamonte* from the Shibantan Member, Denying Formation near Jiulongwan, Hubei (Meyer *et al*., 2014); (L) Cambrian black shale of Shuijingtou Formation with trilobite *Tsunydiscus* near Taishanmiao, Hubei (Zhang *et al*., 2020).

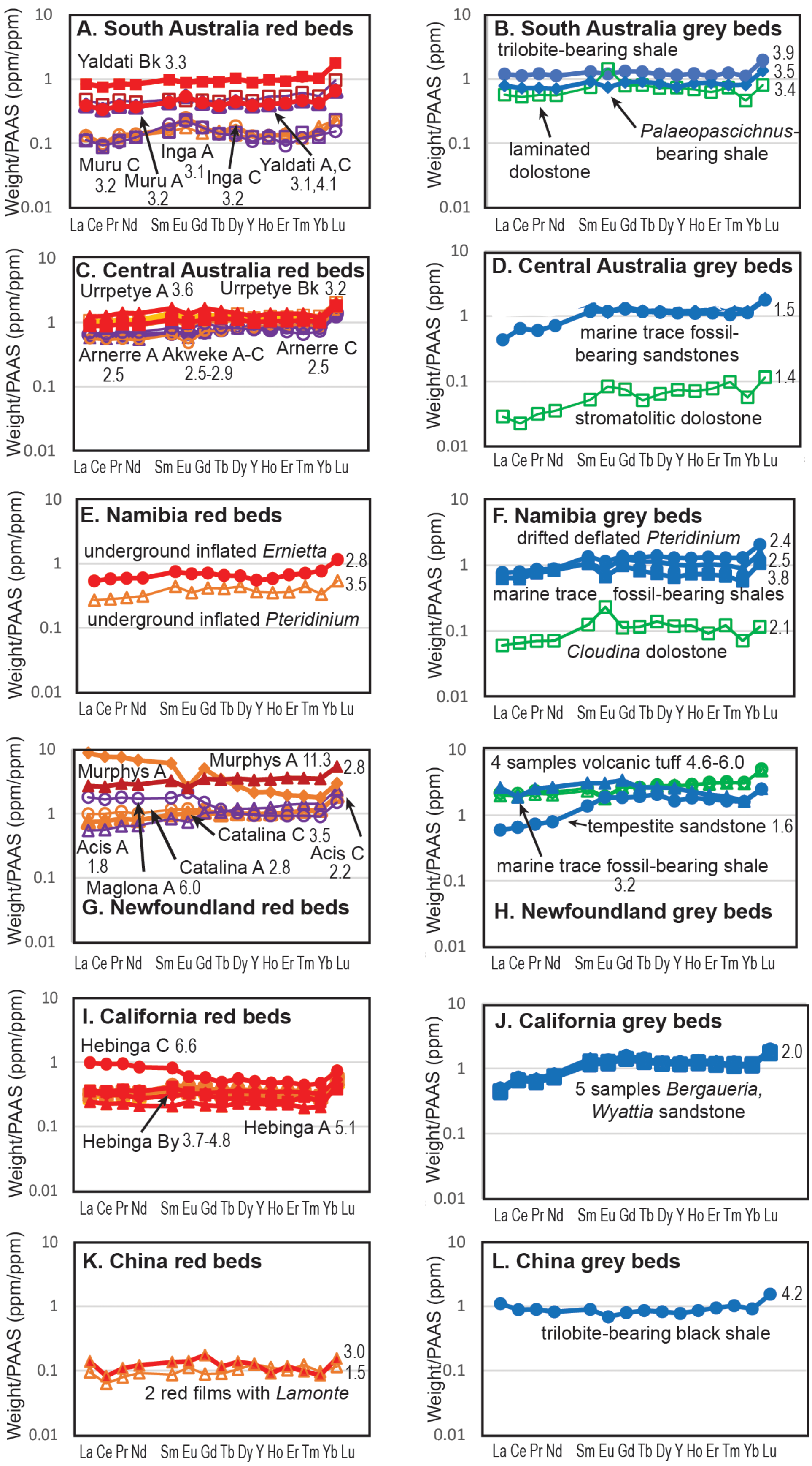
A. South Australia red beds
Yaldati Bk 3.3
Inga A
Muru C 3.2
Muru A 3.2
3.1
Inga C 3.2
Yaldati A,C 3.1,4.1
B. South Australia grey beds
trilobite-bearing shale
3.9
3.5
3.4
laminated dolostone
Palaeopascichnus-bearing shale
C. Central Australia red beds
Urrpetye A 3.6
Urrpetye Bk 3.2
Arnerre A 2.5
Akweke A-C 2.5-2.9
Arnerre C 2.5
D. Central Australia grey beds
marine trace fossil-bearing sandstones
1.5
1.4
stromatolitic dolostone
E. Namibia red beds
underground inflated *Ernietta*
2.8
3.5
underground inflated *Pteridinium*
F. Namibia grey beds
drifted deflated *Pteridinium*
2.4
2.5
3.8
marine trace fossil-bearing shales
2.1
Cloudina dolostone
Murphys A
Murphys A 11.3
2.8
Catalina C 3.5
Acis A 1.8
Catalina A 2.8
Acis C 2.2
Maglona A 6.0
G. Newfoundland red beds
4 samples volcanic tuff 4.6-6.0
tempestite sandstone 1.6
marine trace fossil-bearing shale 3.2
H. Newfoundland grey beds
I. California red beds
Hebinga C 6.6
Hebinga By 3.7-4.8
Hebinga A 5.1
J. California grey beds
2.0
5 samples *Bergaueria*, *Wyattia* sandstone
K. China red beds
3.0
1.5
2 red films with *Lamonte*
L. China grey beds
4.2
trilobite-bearing black shale
Weight/PAAS (ppm/ppm)
Weight/PAAS (ppm)
10
1
0.1
0.01
La Ce Pr Nd Sm Eu Gd Tb Dy Y Ho Er Tm Yb Lu

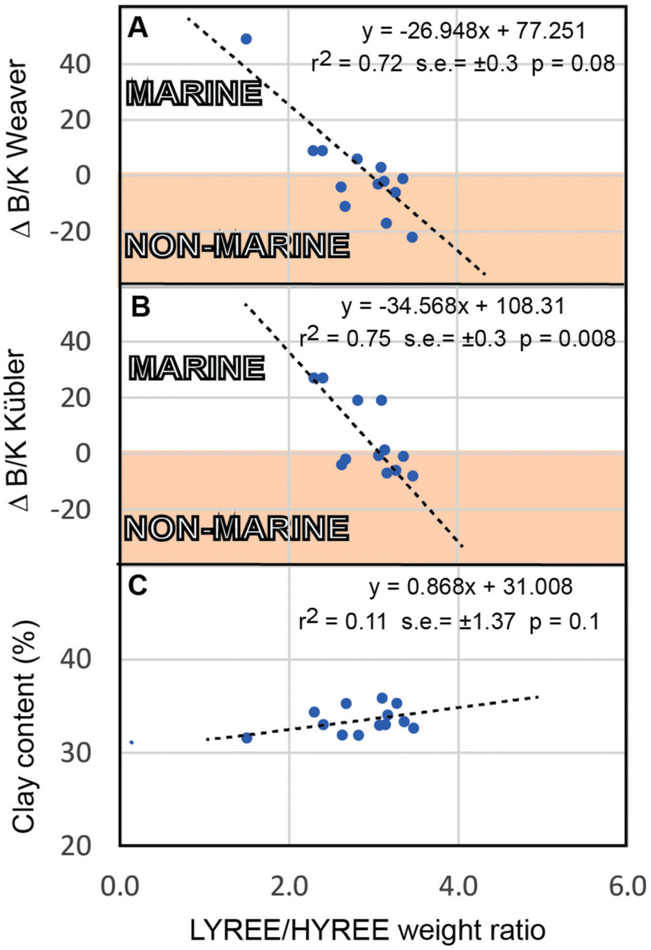

Fig. 10—Comparison of LYREE/HYREE weight ratios with boron proxies for paleosalinity and weight percent clay in 13 samples analyzed also by Retallack (2020). $\Delta_{B/K}$ Weaver and $\Delta_{B/K}$ Kübler are differences from marine–non–marine threshold adjusted for Weaver and Kübler estimates of diagenesis of clays, which are the main carrier of B in these rocks.

clayey tails of genuine turbidites (Bouma, 1964; Korsch *et al*., 1993). Geochemically, the Newfoundland beds were also very distinct from turbidites (Retallack, 2014, 2016).

EDIACARAN HABITATS AND PALEOCLIMATE

The clearest result of this study is falsification of abyssal marine paleoenvironment for the Ediacaran fossil beds of Newfoundland (Narbonne *et al*., 2014; Liu *et al*., 2015). A tempestite from Newfoundland has marine LYREE/HYREE ratios less than 2.7, but even that is normal for rivers and turbidites derived from volcanic arcs (Fig. 2A). Most Newfoundland beds have higher ratios of shallow marine to terrestrial sediments and intertidal paleosols, and some paleosols and tuffs have clear paleosol values of 6.0–11.3 (Fig. 9G–H). This new result supports a variety of lines of evidence that the surfaces with vendobionts in the Mistaken Point and Drook formations were coastal paleosols (Retallack, 2014, 2016). Supposed animal trails in the Mistaken Point Formation (Liu *et al*., 2010) were thus tilting traces formed in shallow water (Retallack, 2010). The problematic fossil *Haootia* (Liu *et al*., 2014, 2015), with cnidarian affinities disputed by Miranda *et al*. (2015), is more like the modern lichen *Cetraria* (Kärnefelt *et al*., 1993; Pérez–Ortega *et al*., 2012). Mistaken Point fossils are more like communities of plants and lichens than any known benthic marine communities in their unusually high beta diversity (Finnegan *et al*., 2019), vegetative propagation (Mitchell *et al*., 2015), and lack of interspecific interaction (Mitchell *et al*., 2019). Comparable terrestrial habitats for vendobionts from other parts of the world are neither falsified nor strongly supported by flat YREE arrays presented here, but rest on evidence from paleosols (Retallack, 2013, 2019a; Retallack & Broz, 2020), boron content (Retallack, 2020), Ge/Si ratios (Retallack, 2017), and eolian interbeds (Retallack, 2019a; McMahon *et al*., 2020).

Alternation of marine and non–marine facies in Ediacaran sequences can be related to glacial drawdowns of sea level (Fig. 7). The Wonoka Paleocanyons of South Australia are evidence of least 600 m of sea level drawdown (Retallack *et al*., 2014) during deposition of Bou Azzer tillites in Morocco now dated to 565 Ma (Linneman *et al*., 2018), which is also the age of Mistaken Point Formation red beds in the otherwise marine continental forearc basin of Newfoundland (Retallack, 2016). Each of four named glaciations during the Ediacaran are also reflected in carbonate carbon isotopic chemostratigraphy (Fig. 7; Xiao & Narbonne, 2020), because meteoric weathering during low stands of the sea imparts a very low carbon isotopic composition (Retallack *et al*., 2014, 2021). Ediacaran paleoclimate was generally cool with a chance of icebergs, and Ediacaran paleosol paleothermometers return temperate values even in tropical paleolatitudes (Retallack, 2013, 2016; Retallack & Broz, 2020). Fluid inclusion homogenization temperatures of Ediacaran halites are evidence of tropical seawater temperatures of only 23.1 ± 5°C (Meng *et al*., 2011), and cool tropical waters also are indicated by relatively high $\delta^{18}O$ values of Ediacaran marine carbonates (Tahata *et al*., 2013). Ikaite pseudomorphs (glendonites) indicative of cold (–1.9 °C to +3 °C) marine waters have been reported from low paleolatitude Ediacaran rocks of China (Wang *et al*., 2017).

The Ediacaran Period was not a permanent paleoclimatic reversal of Cryogenian "Snowball Earth", which itself may have been the result of biologically enhanced weathering on land with evolution of fungi and other eukaryotes replacing largely prokaryotic microbiomes (Lenton & Watson, 2004; Retallack, 2021b, 2023; Retallack *et al*., 2021). Observed evolutionary increases in size and complexity of Ediacaran vendobionts culminating in large *Dickinsonia* and *Arumberia* interpreted as terrestrial vegetation in paleosols (Retallack, 2013; Retallack & Broz, 2020), may have triggered additional glacial advances punctuating the Ediacaran Period (Hebert *et al*., 2010; Linneman *et al*., 2018; Retallack, 2021a).

CONCLUSIONS

YREE arrays have long been used to determine provenance and general composition of source areas of sedimentary rocks (Taylor & McLennan, 1985). LYREE/HYREE ratios also have been used to distinguish Precambrian marine from non–marine depositional environments, most effectively in chemical sediments (Bolhar *et al*., 2004, 2005). The approach employed here to minimize provenance effects in siliciclastic sediments is to use of weight ratios, as a reflection of marine versus non–marine complexation in proportion to atomic number (Ronov *et al*., 1967; Duddy, 1980), and to compare different samples of the same provenance.

Ediacaran red beds, and some grey beds from Newfoundland, China, Namibia, and Australia showed ambiguously continental terrestrial or very shallow marine arrays with modest light YREE enrichment. A grey tempestite from Newfoundland, a grey sandstone from California, and grey carbonates from Australia and Namibia showed clear oceanic arrays with heavy YREE enrichment. Vendobiont fossils such as *Dickinsonia*, *Spriggina*, *Ernietta* and *Pteridinium* have flat YREE patterns undiagnostic of marine or terrestrial, although other evidence favours terrestrial (Retallack, 2013, 2020, 2022a). However, *Fractofusus* and *Charniodiscus* from Newfoundland show significant light YREE enrichment of paleosols. These vendobionts did not live at abyssal depths in the ocean, but on coastal plains (Retallack, 2014, 2016).

Evidence from YREE falsifies the view that Newfoundland vendobionts were deep marine invertebrates living on dissolved organic matter or sulfide chemosymbiosis (Mitchell *et al*., 2015, 2019), that they were deep water evolutionary precursors of late Ediacaran shallow marine organisms (Narbonne *et al*., 2014), and that they were uprooted by later Ediacaran development of burrowing marine organisms (Briggs, 2015; Wood *et al*., 2019). Evidence from YREE for habitats of other Ediacaran vendobionts are less conclusive, but also compatible with the view that they were instead an early form of terrestrial vegetation in coastal paleosols buried by tsunamite sandstones (Retallack, 2014, 2016). These large creatures would have enhanced weathering and productivity on land, and thus fueled the late Ediacaran and Cambrian explosion of life on the sea (Retallack, 2022a).

Acknowledgements—*Permission to undertake fieldwork in Flinders Ranges National Park was facilitated by K. Lloyd, P. Coulthard, A. Coulthard, K. Anderson and D. Crawford. Fieldwork was funded by the PRF fund of the American Chemical Society, and aided by C. Metzger and J. Gehling. Fieldwork in Newfoundland in 2011 was funded by the University of Oregon, under permit from Siân French Director of Parks and Natural Areas Division of Newfoundland and Labrador, with local aid by Richard Thomas. Fieldwork in China was funded by the Chinese Academy of Sciences for attendance at a 2013 meeting organized by Hongfu Yin in Wuhan. Fieldwork in Namibia was part of an excursion in 2016 led by Patricia Vickers–Rich for the International Geological Congress in Cape Town.*

REFERENCES

Allwood AC, Kamber BS, Walter MR, Burch IW & Kanik I 2010. Trace elements record depositional history of an Early Archean stromatolitic carbonate platform. Chemical Geology 270: 148−163. https://doi.org/10.1016/j.chemgeo.2009.11.01

Anaya–Gregorio A, Armstrong–Altrin JS, Machain–Castillo ML, Montiel–García PC & Ramos–Vázquez MA 2018. Textural and geochemical characteristics of late Pleistocene to Holocene fine–grained deep–sea sediment cores (GM6 and GM7), recovered from southwestern Gulf of Mexico. Journal of Palaeogeography 7: 1−19. https://doi.org/10.1186/s42501–018–0005–3

Bau M 1996. Controls on the fractionation of isovalent trace elements in magmatic and aqueous systems: evidence from Y/Ho, Zr/Hf, and lanthanide tetrad effect. Contributions to Mineralogy and Petrology 123: 323−333. https://doi.org/10.1007/s00410005015

Bayon G, Toucanne S, Skonieczny C, André L, Bermell S, Cheron S, Dennielou B, Etoubleau J, Freslon N, Gauchery T & Germain Y 2015. Rare earth elements and neodymium isotopes in world river sediments revisited. Geochimica et Cosmochimica Acta 170: 17−38. https://dx.doi.org/10.1016/j.gca.2015.08.001

Berner RA & Raiswell R 1984. C/S method for distinguishing freshwater from marine sedimentary rocks. Geology 12: 365−368. https://doi.org/10.1130/0091−7613(1984)12<365: CMFDFF>2.0.C

Beyth M, Stern RJ, Altherr R & Kröner A 1994. The late Precambrian Timna igneous complex, southern Israel: evidence for comagmatic–type sanukitoid monzodiorite and alkali granite magma. Lithos 31: 103−124. https://doi.org/10.1016/0024–4937(94)90003–5

Bolhar R, Kamber BS, Moorbath S, Fedo CM & Whitehouse MJ 2004. Characterisation of early Archaean chemical sediments by trace element signatures. Earth and Planetary Science Letters 222: 43−60. https://doi.org/10.1016/j.epsl.2004.02.0

Bolhar R & Van Kranendonk MJ 2007. A non–marine depositional setting for the northern Fortescue Group, Pilbara Craton, inferred from trace element geochemistry of stromatolitic carbonates. Precambrian Research 155: 229−250. https://doi.org/10.1016/j.precamres.2007.02.0

Bolhar R, Van Kranendonk MJ & Kamber BS 2005. A trace element study of siderite–jasper banded iron formation in the 3.45 Ga Warrawoona Group, Pilbara Craton—formation from hydrothermal fluids and shallow seawater. Precambrian Research 137: 93−114. https://doi.org/10.1016/j.precamres.2005.02.001

Bottjer DJ, Hagadorn JW & Dornbos SQ 2000. The Cambrian substrate revolution. GSA Today 10: 1–7.

Bouma A 1964. Turbidites. Developments in Sedimentology 3: 247−256.

Braun JJ, Viers J, Dupré B, Polve M, Ndam J & Muller JP 1998. Solid/liquid REE fractionation in the lateritic system of Goyoum, East Cameroon: the implication for the present dynamics of the soil covers of the humid tropical regions. Geochimica et Cosmochimica Acta 62: 273−299. https://doi.org/10.1016/S0016–7037(97)00344

Briggs DE 2015. The Cambrian explosion. Current Biology 25: 864−868. https://doi.org/10.1016/j.cub.2015.04.047

Brito P, Prego R, Mil–Homens M, Caçador I & Caetano M 2018. Sources and distribution of yttrium and rare earth elements in surface sediments from Tagus Estuary, Portugal. Science of the Total Environment 621: 317−325. https://doi.org/10.1016/j.scitotenv.2017.11.24

Caccia VG & Millero FJ 2007. Distribution of yttrium and rare earths in Florida Bay sediments. Marine Chemistry 104: 171−185. https://doi.org/10.1016/j.marchem.2006.11.001

Cai Y, Cortijo I, Schiffbauer JD & Hua H 2017. Taxonomy of the late Ediacaran index fossil *Cloudina* and a new similar taxon from South China. Precambrian Research 298: 146−156. https://doi.org/10.1016/j.precamres.2017.05.01

Chen Z, Zhou C, Xiao S, Wang W, Guan C, Hua H & Yuan X 2014. New Ediacara fossils preserved in marine limestone and their ecological implications. Nature Scientific Reports 4: 4180. https://doi.org/10.1038/srep04180

Compton JS, White RA & Smith M 2003. Rare earth element behavior in soils and salt pan sediments of a semi–arid granitic terrain in the Western Cape, South Africa. Chemical Geology 201: 239−255. https://doi.org/10.1016/S0009–2541(03)00239–0

Corsetti FA, Awramik SM, Pierce D & Kaufman AJ 2000. Using chemostratigraphy to correlate and calibrate unconformities in Neoproterozoic strata from the southern Great Basin of the United States. International Geology Review 42: 516–533. https://doi.org/10.1080/00206810009465096

Corsetti FA & Hagadorn JW 2003. The Precambrian–Cambrian transition in the southern Great Basin, USA. The Sedimentary Record 1: 4−8.

Corsetti FA & Kaufman AJ 1994. Chemostratigraphy of Neoproterozoic–Cambrian units, White–Inyo Region, eastern California and western Nevada; implications for global correlation and faunal distribution. Palaios 9: 211–219. https://doi.org/10.2307/351510

Das BK, Gaye B & Kaur P 2008. Geochemistry of Renuka Lake and wetland sediments, Lesser Himalaya (India): implications for source–area weathering, provenance, and tectonic setting. Environmental Geology 54: 147−163. https://doi.org/10.1007/s00254–007–0801–z

Das BK & Haake BG 2003. Geochemistry of Rewalsar Lake sediment, Lesser Himalaya, India: implications for source–area weathering, provenance and tectonic setting. Geoscience Journal 7: 299−312. https://doi.org/10.1007/BF02919560

Davies G & Woodroffe CD 2010. Tidal estuary width convergence: theory and form in North Australian estuaries. Earth Surface Processes and Landforms 35: 737−749. https://doi.org/10.1002/esp.1864

Davies NS, Gibling MR & Rygel MC 2011. Alluvial facies evolution during the Palaeozoic greening of the continents: case studies, conceptual models and modern analogues. Sedimentology 58: 220−258. https://doi.org/10.1111/j.1365–3091.2010.01215.x

Dias AS & Barriga FJ 2006. Mineralogy and geochemistry of hydrothermal sediments from the serpentinite–hosted Saldanha hydrothermal field (36 34′ N; 33 26′ W) at MAR. Marine Geology 225: 157−175. https://doi.org/10.1016/j.margeo.2005.07.01

dos Santos JCB, Le Pera E, de Oliveira CS, de Souza Junior VS, de Araújo Pedron F, Corrêa MM & de Azevedo AC 2019. Impact of weathering on REE distribution in soil–saprolite profiles developed on orthogneisses in Borborema Province, NE Brazil. Geoderma 347: 103−117. https://doi.org/10.1016/10.1016/j.geoderma.2019.03.04

Duddy LR 1980. Redistribution and fractionation of rare–earth and other elements in a weathering profile. Chemical Geology 30: 363−381. https://doi.org/10.1016/0009–2541(80)90102–3

Fedo CM & Cooper J D 2001. Sedimentology and sequence stratigraphy of Neoproterozoic and Cambrian units across a craton–margin hinge zone, southeastern California, and implications for the early evolution of the Cordilleran margin. Sedimentary Geology 141: 501–522. https://doi.org/10.1016/S0037–0738(01)00088

Fedonkin MA, Gehling JG, Grey K, Narbonne GM & Vickers–Rich P 2008. The Rise of Animals: Evolution and Diversification of the Kingdom Animalia. Johns Hopkins University Press, Baltimore, 344 p.

Finnegan S, Gehling JG & Droser ML 2019. Unusually variable paleocommunity composition in the oldest metazoan fossil assemblages. Paleobiology 45: 235−245. https://doi.org/10.1017/pab.2019.1

Fowler AD & Doig R 1983. The significance of europium anomalies in the REE spectra of granites and pegmatites, Mont Laurier, Quebec. Geochimica et Cosmochimica Acta 47: 1131−1137. https://doi.org/10.1016/0016–7037(83)90243–0

Garcia D, Joseph P, Maréchal B & Moutte J 2004. Patterns of geochemical variability in relation to turbidite facies in the Grès d'Annot Formation. *In*: Joseph P & Lomas SA (Editors)− Deep–Water Sedimentation in the Alpinje Zone of SE France: new perspectives on the Grès d'Arnot and related systems. Special Publication Geological Society of London 221: 349−365.

Gehling JG 2000. Environmental interpretation and a sequence stratigraphic framework for the terminal Proterozoic Ediacara Member within the Rawnsley Quartzite, South Australia. Precambrian Research 100: 65–95. https://doi.org/10.1016/S0301–9268(99)00069–

Gehling GJ & Droser ML 2013. How well do fossil assemblages of the Ediacara Biota tell time? Geology 41: 447–450. https://doi.org/10.1130/G33881.1

Glaessner MF & Walter MR 1975. New Precambrian fossils from the Arumbera Sandstone, Northern Territory, Australia. Alcheringa 1: 59−69. https://doi.org/10.1080/03115517508619480

Grazhdankin D & Seilacher A 2002. Underground Vendobionta from Namibia. Palaeontology 45: 57−78, https://doi.org/10.1111/1475–4983.00227.

Hagadorn JW, Fedo M & Waggoner B 2000. Early Cambrian Ediacaran–type fossils from California. Journal of Paleontology 74: 731–740. https://doi.org/10.1666/0022–3360(2000)074<0731: ECETFF>2.0.CO;2

Harlavan Y, Erel Y & Blum JD 2009. The coupled release of REE and Pb to the soil labile pool with time by weathering of accessory phases, Wind River Mountains, WY. Geochimica et Cosmochimica Acta 73: 320−336. https://doi.org/10.1016/j.gca.2008.11.002

Hebert CL, Kaufman AJ, Penniston–Dorland SC & Martin AJ 2010. Radiometric and stratigraphic constraints on terminal Ediacaran (post–Gaskiers) glaciation and metazoan evolution. Precambrian Research 182: 402−412. https://doi.org/ 10.1016/j.precamres.2010.07.008

Hongo Y & Nozaki Y 2001. Rare earth element geochemistry of hydrothermal deposits and Calyptogena shell from the Iheya Ridge vent field, Okinawa Trough. Geochemical Journal 35: 347−354. https://doi.org/10.2343/geochemj.35.347

Hu X–M 2013. Distribution, types and origins of Phanerozoic marine red beds. Bulletin of Mineralogy Petrology and Geochemistry 32: 355−342. http://www.bmpg.ac.cn/CN/Y2013/V32/I3/335

Ichaso AA, Dalrymple RW & Narbonne GM 2007. Paleoenvironmental and basin analysis of the late Neoproterozoic (Ediacaran) upper Conception and St. John's Groups, west Conception Bay, Newfoundland. Canadian Journal of Earth Sciences 44: 25–41. https://doi.org/10.1139/e06–09

Ivantsov AY, Narbonne GM, Trusler PW, Greentree C & Vickers–Rich P 2016. Elucidating *Ernietta*: new insights from exceptional specimens in the Ediacaran of Namibia. Lethaia 49: 540−554. https://doi.org/10.1111/let.12164

Jaireth S, Hoatson DM & Miezitis Y 2014. Geological setting and resources of the major rare–earth–element deposits in Australia. Ore Geology Reviews 62: 72−128. https://doi.org/10.1016/j.oregeorev.2014.02.00

Jenkins RJF, Ford CH & Gehling JG 1983. The Ediacara Member of the Rawnsley Quartzite: the context of the Ediacara assemblage (late Precambrian, Flinders Ranges). Geological Society of Australia Journal 30: 101–119. https://doi.org/10.1080/00167618308729240

Jensen S, Gehling JG & Droser ML 1998. Ediacara–type fossils in Cambrian sediments. Nature 393: 567−569. https://doi.org/10.1038/31215

Kärnefelt I, Mattsson JE & Thell A 1993. The lichen genera *Arctocetraria*, *Cetraria*, and *Cetrariella* (Parmeliaceae) and their presumed evolutionary affinities. Bryologist 96: 394–404. https://doi.org/10.2307/3243869

Kiminami K & Fujii K 2007. The relationship between major element concentration and grain size within sandstones from four turbidite sequences in Japan. Sedimentary Geology 195: 203−215. https://doi.org/10.1016/j.sedgeo.2006.08.002

King AF 1988. Geology of the Avalon Peninsula, Newfoundland: St Johns, Newfoundland, Newfoundland Department of Mines Map 88–01, scale 1: 250,000.

Korsch RJ, Roser BP & Kamprad JL 1993. Geochemical, petrographic and grain–size variations within single turbidite beds. Sedimentary Geology 83: 15−35. https://doi.org/ 10.1016/0037–0738(93)90180–

Lee JH & Byrne RH 1992. Complexation of trivalent rare earth elements (Ce, Eu, Gd, Tb, Yb) by carbonate ions. Geochimica et Cosmochimica Acta 57: 295–302. https://doi.org/ 10.1016/0016–7037(93)90432–

Lenton TM & Watson AJ 2004. Biotic enhancement of weathering, atmospheric oxygen and carbon dioxide in the Neoproterozoic. Geophysical Research Letters 31: L05202. https://doi.org/10.1029/2003GL018802

Ling H–F, Chen X, Li D–A, Wang D, Shields–Zhou GA & Zhu M 2013. Cerium anomaly variations in Ediacaran–earliest Cambrian carbonates from the Yangtze Gorges area, South China: implications for oxygenation of coeval shallow seawater. Precambrian Research 225: 110−127. https://doi.org/10.1016/j.precamres.2011.10.011

Linnemann U, Pidal AP, Hofmann M, Drost K, Quesada C, Gerdes A, Marko L, Gärtner A, Zieger J, Ulrich J, Krause R, Vickers–Rich P & Horak J 2018. A~565 Ma old glaciation in the Ediacaran of peri–Gondwanan West Africa. International Journal of Earth Science 107: 885−911. https://doi.org/10.1007/s00531–017–1520–7

Liu AG, Kenchington CG & Mitchell EG 2015. Remarkable insights into the paleoecology of the Avalonian Ediacaran macrobiota. Gondwana Research 27: 1355−1380. https://doi.org/10.1016/j.gr.2014.11.002

Liu AG, Matthews JJ, Menon LR, McIlroy D & Brasier MD 2014. *Haootia quadriformis* n. gen., n. sp., interpreted as a muscular cnidarian impression from the Late Ediacaran period (approx. 560 Ma). Proceedings of the Royal Society B281: 20141202. https://doi.org/10.1098/rspb.2014.1202

Liu AG, Matthews JJ, Menon LR, McIlroy D & Brasier MD 2015. The arrangement of possible muscle fibres in the Ediacaran taxon *Haootia quadriformis*. Proceedings of the Royal Society B282: 2014294. https://doi.org/10.1098/rspb.2014.2949

Liu AG, Mcllroy D & Brasier MD 2010. First evidence for locomotion in the Ediacara biota from the 565 Ma Mistaken Point Formation, Newfoundland. Geology 38: 123−126. https://doi.org/10.1130/G30368.1

Mángano MG, Buatois LA, Waisfeld BG, Muñoz DF, Vaccari NE & Astini RA 2021. Were all trilobites fully marine? Trilobite expansion into brackish water during the early Palaeozoic. Proceedings of the Royal Society B288: 2020.2263. https://doi.org/10.1098/rspb.2020.2263

Mawson D & Segnit ER 1949. Purple slates of the Adelaide System. Transactions of the Royal Society of South Australia 72: 276–280.

McLennan SM 1989. Rare earth elements in sedimentary rocks: influence of provenance and sedimentary processes. *In*: Lipin BR & McKay GA (Editors) − Geochemistry and mineralogy of rare earth elements, v. 21. Walter de Gruyter, Berlin, p.169−200.

McLennan SM, Taylor SR, McCulloch MT & Maynard JB 1990. Geochemical and Nd–Sr isotopic composition of deep–sea turbidites: crustal evolution and plate tectonic associations. Geochimica et Cosmochimica Acta 54: 2015−2050. https://doi.org/ 10.1016/0016–7037(90)90269–Q

McMahon WJ, Davies NS, Liu AG & Went DJ 2022. Enigma variations: characteristics and likely origin of the problematic surface texture *Arumberia*, as recognized from an exceptional bedding plane exposure and the global record. Geological Magazine 159: 1−20. https://doi.org/10.1017/S0016756821000777

McMahon WJ, Liu AG, Tindal BH & Kleinhans MG 2020. Ediacaran life close to land: Coastal and shoreface habitats of the Ediacaran macrobiota, the Central Flinders Ranges, South Australia. Journal of Sedimentary Research 90: 1463−1499. https://doi.org/10.2110/jsr.2020.029

Meng F, Ni P, Schiffbauer JD, Yuan X, Zhou C, Wang Y & Xia M 2011. Ediacaran seawater temperature: evidence from inclusions of Sinian halite. Precambrian Research 184: 63−69. https://doi.org/10.1016/j.precamres.2010.10.004

Meyer M, Xiao S, Gill BC, Schiffbauer JD, Zhe C, Zhou C & Yuan X 2014. Interactions between Ediacaran animals and microbial mats: Insights from *Lamonte trevallis*, a new trace fossil from the Dengying Formation of South China. Palaeogeography Palaeoclimatology Palaeoecology 396: 62−74. https://doi.org/10.1016/j.palaeo.2013.12.026

Michard A & Alberede F 1986. The REE content of some hydrothermal fluids. Chemical Geology 55: 51−60. https://doi.org/10.1016/10.1016/0009–2541(86)90127–0

Minařík L, *Žigová* A, Bendl J, Skřivan P & *Štástnýd* M 1998. The behaviour of rare–earth elements and Y during the rock weathering and soil formation in the Říčany granite massif, Central Bohemia. Science of the Total Environment 215: 101−111. https://doi.org/10.1016/S0048–9697(98)00113–2

Miranda LS, Collins AG & Marques AC 2015. Is *Haootia quadriformis* related to extant Staurozoa (Cnidaria)? Evidence from the muscular system reconsidered. Proceedings of the Royal Society B282: 20142396. https://doi.org/10.1098/rspb.2014.2396

Mitchell EG, Kenchington CG, Liu AG, Matthews JJ & Butterfield NJ 2015. Reconstructing the reproductive mode of an Ediacaran macro–organism. Nature 524: 343−346. https://doi.org/10.1038/nature14646

Mitchell EG, Harris S, Kenchington CG, Vixseboxse P, Roberts L, Clark C, Dennis A, Liu AG & Wilby PR 2019. The importance of neutral over niche processes in structuring Ediacaran early animal communities. Ecology Letters 22: 2028−2038. https://doi.org/10.1111/ele.13383

Muhlbauer JG, Fedo CM & Moersch JE 2020. Architecture of a distal pre–vegetation braidplain: Cambrian middle member of the Wood Canyon Formation, southern Marble Mountains, California, USA. Sedimentology 67: 1084−1113. https://doi.org/10.1111/sed.12677

Munemoto T, Solongo T, Okuyama A, Fukushi K, Yunden A, Batbold T, Altansukh O, Takahashi Y, Iwai H & Nagao S 2020. Rare earth element distributions in rivers and sediments from the Erdenet Cu–Mo mining area, Mongolia. Applied Geochemistry 123: 104800. https://doi.org/10.1016/j.apgeochem.2020.104800

Narbonne GM, Laflamme M, Trusler PW, Dalrymple RW & Greentree C 2014. Deep–water Ediacaran fossils from Northwestern Canada: taphonomy, ecology, and evolution. Journal of Paleontology 88: 207−223. https://doi.org/10.1666/13–053

O'Brien SJ, O'Brien BH, Dunning GR & Tucker RD 1996. Late Neoproterozoic Avalonian and related peri–Gondwanan rocks of the Newfoundland Appalachians. *In*: Nance RD & Thompson MD (Editors) − Avalonian and Related Peri–Gondwanan Terranes of the Circum–North Atlantic. Geological Society of America Special Paper 304: 9–28. https://doi.org/10.1130/0–8137–2304–3.9

Paterson JR & Brock GA 2007. Early Cambrian trilobites from Angorichina, Flinders Ranges, South Australia, with a new assemblage from the *Pararaia bunyerooensis* Zone. Journal of Paleontology 81: 116−142. https://doi.org/10.1666/0022–3360(2007)81[116: ECTFAF]2.0.CO2

Pérez–Ortega S, Fernández–Mendoza F, Raggio J, Vivas M, Ascaso C, Sancho LG, Printzen C & de Los Ríos A 2012. Extreme phenotypic variation in *Cetraria aculeata* (lichenized Ascomycota): adaptation or incidental modification? Annals of Botany 109: 1133–1148. https://doi.org/10.1093/aob/mcs042

Peters R, Jaffe B & Gelfenbaum G 2007. Distribution and sedimentary characteristics of tsunami deposits along Cascadia margin of North America. Sedimentary Geology 200: 372–386. https://doi.org/10.1016/j.sedgeo.2007.01.01

Retallack GJ 2010. First evidence for locomotion in the Ediacara biota from the 565 Ma Mistaken Point Formation, Newfoundland: Comment. Geology 38: e223−e223. https://doi.org/10.1130/G31137C.1

Retallack GJ 2011. Neoproterozoic loess and limits to Snowball Earth. Journal of the Geological Society of London 168: 289−308. https://doi.org/10.1144/0016–76492010–051

Retallack GJ 2013. Ediacaran life on land. Nature 493: 89−92. https://doi.org/10.1038/nature11777

Retallack GJ 2014. Volcanosedimentary paleoenvironments of Ediacaran fossils in Newfoundland. Geological Society of America Bulletin 126: 619−638. https://doi.org/10.1130/B30892.1

Retallack GJ 2016. Ediacaran sedimentology and paleoecology of Newfoundland reconsidered. Sedimentary Geology 333: 15−31. https://doi.org/ 10.1016/j.sedgeo.2015.12.001

Retallack GJ 2017. Exceptional preservation of soft–bodied Ediacara Biota promoted by silica–rich oceans: comment. Geology 45: e407. https://doi.org/10.1130/G38763C.1

Retallack GJ 2018. Reassessment of the Devonian problematicum

Protonympha as another post–Ediacaran Vendobiont. Lethaia 51: 406–423. https://doi.org/10.1111/let.1225

Retallack GJ 2019a. Interflag sandstone laminae, a novel sedimentary structure, with implications for Ediacaran paleoenvironments. Sedimentary Geology 379: 60–76. https://doi.org/10.1016/j.sedgeo.2018.11.003

Retallack GJ 2019b. Ordovician land plants and fungi from Douglas Dam, Tennessee. The Palaeobotanist 68: 173–205. https://doi.org/10.54991/jop.2019.43

Retallack GJ 2020. Boron paleosalinity proxy for deeply buried Paleozoic and Ediacaran fossils. Palaeogeography Palaeoclimatology Palaeoecology 540: 109536. https://doi.org/10.1016/j.palaeo.2019.109536

Retallack GJ 2021a. Towards a glacial subdivision of the Ediacaran Period, with example of the Boston Bay Group, Massachusetts. Australian Journal of Earth Sciences 69: 223–250. https://doi.org/10.1080/08120099.2021.1954088

Retallack GJ 2021b. Paleosols and weathering leading up to Snowball Earth in central Australia. Australian Journal of Earth Sciences 68: 1122–1148. https://doi.org/10.1080/08120099.2021.1906747

Retallack GJ 2022a. Biotic enhancement of weathering over the past 3.7 billion years. GSA Today 32: 4–9. https://doi.org/10.1130/GSATG543A.1

Retallack GJ 2022b. Reconsideration of the Ediacaran problematicum *Aulozoon*. Journal of Palaeosciences 71: 143–157. https://doi.org/10.54991/jop.2022.1284.

Retallack GJ 2023. Why was there a Neoproterozoic Snowball Earth? Precambrian Research 385: 106952. https://doi.org/10.1016/j.precamres.2022.106952

Retallack GJ & Broz AP 2020. Ediacaran and Cambrian paleosols from central Australia. Palaeogeography Palaeoclimatology Palaeoecology 560: 110047.

Retallack GJ & Broz AP 2021. *Arumberia* and other Ediacaran–Cambrian fossils of central Australia. Historical Biology 33: 1964–1988. https://doi.org/10.1080/08912963.2020.1755281

Retallack GJ, Broz AP, Lai LSH & Gardner K 2021. Neoproterozoic marine chemostratigraphy, or eustatic sea level change? Palaeogeography Palaeoclimatology Palaeoecology 562: 110155. https://doi.org/10.1016/j.palaeo.2020.110155

Retallack GJ, Marconato A, Osterhout JT, Watts KE & Bindeman IN 2014. Revised Wonoka isotopic anomaly in South Australia and Late Ediacaran mass extinction. Journal of the Geological Society of London 171: 709–722. https://doi.org/10.1144/jgs2014–016

Révillon S, Jouet G, Bayon G, Rabineau M, Dennielou B, Hémond C & Berné S 2011. The provenance of sediments in the Gulf of Lions, western Mediterranean Sea. Geochemistry Geophysics Geosystems 12: GC003523. https://doi.org/10.1029/2011GC003523

Rongemaille E, Bayon G, Pierre C, Bollinger C, Chu NC, Fouquet Y, Riboulot V & Voisset M 2011. Rare earth elements in cold seep carbonates from the Niger Delta. Chemical Geology 286: 196–206. https://doi.org/10.1016/j.chemgeo.2011.05.001

Ronov AB, Balashov YA & Migdisov AA 1967. Geochemistry of the rare earths in the sedimentary cycle. Geochemistry International 4: 1–17.

Roy PD & Smykatz–Kloss W 2007. REE geochemistry of the recent playa sediments from the Thar Desert, India: an implication to playa sediment provenance. Geochemistry 67: 55–68. https://doi.org/10.1016/j.chemer.2005.01.006

Runnegar B 2022. Following the logic behind biological interpretations of the Ediacaran biotas. Geological Magazine 159: 1093–1117. https://doi.org/10.1017/S0016756821000443

Sanematsu K, Murakami H, Watanabe Y, Duangsurigna S & Siphandone V 2009. Enrichment of rare earth elements (REE) in granitic rocks and their weathered crusts in central and southern Laos. Bulletin of the Geological Survey of Japan 60: 527–558. https://doi.org/10.9795/bullgsj.60.527

Seilacher A 1992. Vendobionta and Psammocorallia: lost constructions of Precambrian evolution. Journal of the Geological Society of London 149: 607–613. https://doi.org/10.1144/gsjgs.149.4.0607

Seilacher A, Grazhdankin D & Legouta A 2003. Ediacaran biota: the dawn of animal life in the shadow of giant protists. Paleontological Research 7(1): 43–54. https://doi.org/10.2517/prpsj.7.43

Selly T, Schiffbauer JD, Jacquet SM, Smith EF, Nelson LL, Andreasen BD, Huntley JW, Strange MA, O'Neil GR, Thater CA & Bykova N 2020. A new cloudinid fossil assemblage from the terminal Ediacaran of Nevada, USA. Journal of Systematic Palaeontology 18: 357–379. https://doi.org/10.1080/14772019.2019.1623333

Sholkovitz ER, Landing WM & Lewis BL 1994. Ocean particle chemistry: the fractionation of rare earth elements between suspended particles and seawater. Geochimica et Cosmochimica Acta 58: 1567–1579. https://doi.org/10.1016/0016–7037(94)90559–2

Singh TD & Manikyamba C 2020. Platinum group element geochemistry and whole–rock systematics of the Vempalle sills, Cuddapah Basin, India: Implications on sulphur saturation history, mantle processes, and tectonic setting. Geological Journal 55: 1300–1319. https://doi.org/10.1002/gj.3459

Smith EF, Nelson LL, Strange MA, Eyster AE, Rowland SM, Schrag DP & Macdonald FA 2016. The end of the Ediacaran: Two new exceptionally preserved body fossil assemblages from Mount Dunfee, Nevada, USA. Geology 44: 911–914. https://doi.org/10.1130/G38157.

Smith EF, Nelson LL, Tweedt SM, Zeng H & Workman JB 2017. A cosmopolitan late Ediacaran biotic assemblage: new fossils from Nevada and Namibia support a global biostratigraphic link. Proceedings of the Royal Society of London B284: 20170934. https://doi.org/10.1098/rspb.2017.0934

Strother PK & Foster C 2021. A fossil record of land plant origins from charophyte algae. Science 373: 792–796. https://doi.org/10.1126/science.abj2

Sugahara H, Sugitani K, Mimura K, Yamashita F & Yamamoto K 2010. A systematic rare–earth elements and yttrium study of Archean cherts at the Mount Goldsworthy greenstone belt in the Pilbara Craton: Implications for the origin of microfossil–bearing black cherts. Precambrian Research 177: 73–87. https://doi.org/10.1016/j.precamres.2009.10.005

Szczuciński W, Kokociński M, Rzeszewski M, Chagué–Goff C, Cachão M, Goto K & Sugawara D 2012. Sediment sources and sedimentation processes of 2011 Tohoku–oki tsunami deposits on Sendai Plain, Japan—insights from diatoms, nannoliths and grain size distribution. Sedimentary Geology 282: 40–56. https://doi.org/10.1016/j.sedgeo.2012.07.019

Tahata M, Ueno Y, Ishikawa T, Sawaki Y, Murakami K, Han J, Shu D, Li Y, Guo J, Yoshida N & Komiya T 2013. Carbon and oxygen chemostratigraphy of the Yangtze platform, South China: decoding temperature and environmental changes through the Ediacaran. Gondwana Research 23: 333–353. https://doi.org/10.1016/j.gr.2012.04.005

Tarhan LG, Droser ML, Gehling JG & Dzaugis MP 2017. Microbial mat sandwiches and other anactualistic sedimentary features of the Ediacara Member (Rawnsley Quartzite, South Australia): implications for interpretation of the Ediacaran sedimentary record. Palaios 32: 181–194. https://doi.org/10.2110/palo.2016.060

Taylor SR & McLennan SM 1985. The Continental Crust: its Composition and Evolution. Blackwell, Oxford, 312 p.

Tostevin R, Shields GA, Tarbuck GM, He T, Clarkson MO & Wood RA 2016a. Effective use of cerium anomalies as a redox proxy in carbonate–dominated marine settings. Chemical Geology 438: 146–162. https://doi.org/10.1016/j.chemgeo.2016.06.027

Tostevin R, Wood RA, Shields GA, Poulton SW, Guilbaud R, Bowyer F, Penny AM, He T, Curtis A, Hoffmann KH & Clarkson MO 2016b. Low–oxygen waters limited habitable space for early animals. Nature Communications 7: 12818. https://doi.org/10.1038/ncomms12818

Vickers–Rich P, Ivantsov AY, Trusler PW, Narbonne GM, Hall M, Wilson SA, Greentree C, Fedonkin MA, Elliott DA, Hoffmann KH & Schneider GI 2013. Reconstructing *Rangea*: new discoveries from the Ediacaran of southern Namibia. Journal of Paleontology 87: 1–15. https://doi.org/10.1666/12–074R.

Wade M 1969. Medusae from uppermost Precambrian or Cambrian sandstones, central Australia. Palaeontology 12: 351–365.

Wang CS, Hu XM, Huang YJ, Scott RW & Wagreich M 2009. Overview of Cretaceous Oceanic Red Beds (CORBs): a window on global oceanic and climate change. *In*: Hu X, Wang C, Scott RW, Wagreich M & Jansa L (Editors) – Cretaceous Oceanic Red Beds: Stratigraphy, Composition, Origins and Paleoceanographic and Paleoclimatic Significance. Society of Economic Paleontologists and Mineralosts Special Publication 91: 13−33. https://doi.org/10.2110/sepmsp.091.013

Wang XP, Chen Z, Pang K, Zhou CM, Xiao S, Wan B & Yuan XL 2021. *Dickinsonia* from the Ediacaran Dengying Formation in the Yangtze Gorges area, South China. Palaeoworld 30: 602−609. https://doi.org/10.1016/j.palwor.2021.01.002

Wang Z, Wang J, Suess E, Wang G, Chen C & Xiao S 2017. Silicified glendonites in the Ediacaran Doushantou Formation (South China) and their potential paleoclimatic implications. Geology 45: 115–118. https://doi.org/10.1130/G38613.1

Wei W & Algeo TJ 2020. Elemental proxies for paleosalinity analysis of ancient shales and mudrocks. Geochimica et Cosmochimica Acta 287: 341−366. https://doi.org/ 10.1016/j.gca.2019.06.034

Wood DA, Dalrymple RW, Narbonne GM, Gehling JG & Clapham ME 2003. Paleoenvironmental analysis of the late Neoproterozoic Mistaken Point and Trepassey Formations, southeastern Newfoundland. Canadian Journal of Earth Sciences 40: 1375–1391. https://doi.org/10.1139/e03–048

Wood R, Liu AG, Bowyer F, Wilby PR, Dunn FS, Kenchington CG, Cuthill JFH, Mitchell EG & Penny A 2019. Integrated records of environmental change and evolution challenge the Cambrian Explosion. Nature Ecology and Evolution 3: 528−538. https://doi.org/10.1038/s41559–019–0821–6

Wu HP, Jiang SY, Palmer MR, Wei HZ & Yang JH 2019. Positive cerium anomaly in the Doushantuo cap carbonates from the Yangtze platform, South China: implications for intermediate water column manganous conditions in the aftermath of the Marinoan glaciation. Precambrian Research 320: 93−110. https://doi.org/ 10.1016/j.precamres.2018.10.019

Xiao S & Narbonne GM 2020. The Ediacaran Period. *In*: Gradstein FM, Ogg JG, Schmitz MD & Ogg GD (Editors) − Geologic Time Scale 2020. Elsevier, Amsterdam, p. 521−561.

Yang SY, Lim DI, Jung HS & Oh BC 2004. Geochemical composition and provenance discrimination of coastal sediments around Cheju Island in the southeastern Yellow Sea. Marine Geology 206: 41−53. https://doi.org/10.1016/j.margeo.2004.01.005

Yasukawa K, Nakamura K, Fujinaga K, Machida S, Ohta J, Takaya Y & Kato Y 2015. Rare–earth, major, and trace element geochemistry of deep–sea sediments in the Indian Ocean: Implications for the potential distribution of REY–rich mud in the Indian Ocean. Geochemical Journal 49: 621−635. https://doi.org/10.2343/geochemj.2.0361

Zhang K, Zhu XK & Yan B 2015. A refined dissolution method for rare earth element studies of bulk carbonate rocks. Chemical Geology 412: 82−91. https://doi.org/10.1016/j.chemgeo.2015.07.027

Zhang L, Chang S, Khan MZ, Feng Q, Luo C, Steiner M, Forel M–B, Liu K & Clausen S 2020. Influence of palaeo–redox and diagenetic conditions on the spatial distribution of Cambrian biotas: A case study from the upper Shuijingtuo Formation (Cambrian Series 2, Stage 3), Three Gorges area of South China. Palaeogeography Palaeoclimatology Palaeoecology 548: 109696. https://doi.org/10.1016/j.palaeo.2020.109696

Zhuravlev AY, Wood RA & Penny AM 2015. Ediacaran skeletal metazoan interpreted as a lophophorate. Proceedings of the Royal Society London B282: 20151860. https://doi.org/10.1098/rspb.2015.1860